Supporting Information (99 pages)

Single-Crystal Dynamic Covalent Organic Frameworks for Adaptive Guest Alignments

Shan Liu,[†] Lei Wei,[†] Tengwu Zeng,[†] Wentao Jiang,[†] Yu Qiu,[†] Xuan Yao,[†] Qisheng Wang,[‡] Yingbo Zhao,[†] and Yue-Biao Zhang*,[†]

[†]School of Physical Science and Technology, Shanghai Key Laboratory of High-Resolution Electron Microscopy, State Key Laboratory of Advanced Medical Materials and Devices, ShanghaiTech University, Shanghai 201210, China.

[‡]Shanghai Synchrotron Radiation Facility, Shanghai Advanced Research Institute, Chinese Academic of Sciences, Shanghai 201210, China

Corresponding authors: zhangyb@shanghaitech.edu.cn

Table of Contents

Section 1. Materials preparation and characterization

Materials. The purchased 1.5 g of tetra-(*p*-aminophenyl)-methane (TAM) was placed in a 250 mL round-bottomed flask. Then, 100 mL of tetrahydrofuran (THF) and 10 g of Raney nickel (containing water) were added to the flask. While stirring, 2 g (1.93 mL) of hydrazine hydrate was added in a fume hood, and the solvent began to boil and foam. After the bubbles disappeared, the mixture was heated to reflux at 80 °C for at least three hours. After heating, the clarified THF solution of TAM was obtained by removing the Raney nickel through suction filtration. While the THF was cooling, n-hexane was slowly added until numerous white solids precipitated on the bottle wall. After standing overnight, the solvent in the bottle was decanted, and the remaining white solid was the purified product. The product was spin-dried and dried before use. The remaining Raney nickel in the bottle can be burned after the solvent has evaporated and removed. For single crystal synthesis, purified TAM was used.

Synthesis of COF-300-DC. Terephthalaldehyde (TPA, 12.0 mg, 0.089 mmol) is dissolved in 1,4-dioxane (0.5 mL), added with aniline (0.12 mL, 15 equiv.) and aqueous acetic acid (AcOH; 6 mol L^{-1}, 0.2 mL), resulting in white color flack crystal precipitated out at the bottom of the glass diffusion tube (inner diameter ~4.24 mm) standing vertically. Then, solution of TAM (20.0 mg, 0.052 mmol) dissolved in 1,4-dioxane (0.5 mL, ultra-dry) was then added drop by drop onto the first layer to form stratification. Diffusion control of crystal growth yields prismatic crystals of COF-300 with the size of ~ 50 μm within 6 days. To completely remove high-boiling solvents (dioxane) and keep the framework from collapsing, we used solvent exchange methods to completely remove the guest molecules in the framework and maintain the consistency of the sample crystal. THF, a low-boiling solvent, is used to exchange dioxane for 3 times one day and rocked on a shaker for 3 days.

Synthesis of COF-300-MC. According to reported literature, a vial was added with TPA (12.0 mg, 0.089 mmol), aniline (0.12 mL, 15 equiv.), and 0.5 mL of 1,4-dioxane, and 0.2 mL of AcOH (6 M) to the solution successively. Then TAM (20.0 mg, 0.052 mmol) dissolved in 1,4-dioxane (0.5 mL, ultra-dry) was added to the vial. The mixture was placed at 25 °C and the single crystals of COF-300 slowly crystallized out at room temperature (RT) and the crystal size reached ~40 μm within 30 days, and 60 μm within 60 days. The single crystals were cleaned via the solvent exchange method.

Synthesis of COF-300-VC. Monomer addition order is the same as COF-300-EC, while the vials were wrapped with perforated parafilm, allowing the original solution to volatilize gradually at the beginning reaction. Finally, single crystals grew to 50 μm within 14 days. The single crystals were cleaned via the solvent exchange method.

Size and Morphology Control of COF-300 Single Crystals for *in-situ* Powder X-Ray Diffraction (PXRD) Analyses. To enhance adsorption kinetics while obtaining a large quantity of samples with uniform size and morphology, we utilized the ventilation-vial synthetic protocol. A 20-mL vial was added with TPA (60.0 mg) and 1,4-dioxane (1 mL, ultra-dry), and aniline (0.20 mL), and 1 mL of AcOH (6 M) to the solution successively. Then TAM (100.0 mg) dissolved in 1,4-dioxane (5 mL, ultra-dry) was added to the vial. The mixture was placed at 65 ºC and placed for 5 days. The single crystals (COF-300-10μm) were cleaned via the solvent exchange method using 1,4-dioxane and THF. The phase purity and crystallinity of samples were determined with a powder X-ray diffractometer (PXRD, Bruker, D8 advance, Cu Kα). The crystal size and morphology were examined using a scanning electron microscope (SEM, JEOL, JSM 7800F Prime).

Instrumentation. Fourier-transformed infrared (FT-IR) spectra were collected on a PerkinElmer ALPHA's Platinum ATR FT-IR spectrometer equipped with a single reflection diamond ATR module. Thermogravimetric analyses (TGA) were conducted on a PerkinElmer TGA 8000 instrument with a heating rate of 5 °C·min^{-1} under N_2 flow. Powder X-ray diffraction (PXRD) patterns were collected on a Bruker D8 advance diffractometer operated at 40 kV voltage and 40 mA current with Cu K α radiation (λ = 1.5418 Å) and the patterns were collected in the range of 5-30º (2 θ) with the steps of 0.02º. Samples were held in a monocrystalline silicon sample stage and kept spinning during the measurement. Solid-state ^{13}C nuclear magnetic resonance (SSNMR) spectra were acquired on Bruker Advance III HD 400WB (9.4 T) spectrometer operating at 400.2 MHz for ^{1}H and 100.6 MHz for ^{13}C, at a spinning speed of 10-20 kHz on a 3.2 mm CP MAS probe. The morphology of COF-300-10 μm was examined using a JEOL JSM 7800F Prime scanning electron microscope (SEM).

Solid-state NMR spectroscopy. Solid-state ^{1}H→^{13}C cross polarization (CP) magic angle spinning (MAS) NMR and polarization inverse (CPPI) experiments were performed at 25 °C. Activated samples were packed into zirconia rotors inside a glove box under nitrogen. CP spectra were acquired under dry air with ^{1}H π/2 pulse of 2.3 μs, a contact time of 3 ms and a recycle time of 2 s. High-power ^{1}H decoupling was carried out

using SPINAL64 with a typical field strength of 75 or 86 kHz. For ^{13}C CP MAS NMR spectra of hydrated COF-300-MC, -VC, and -DC, the samples were first activated at 120 °C for 12 hours and then prepared by fumigation of H_2O vapor at 40 °C for 24 hours.

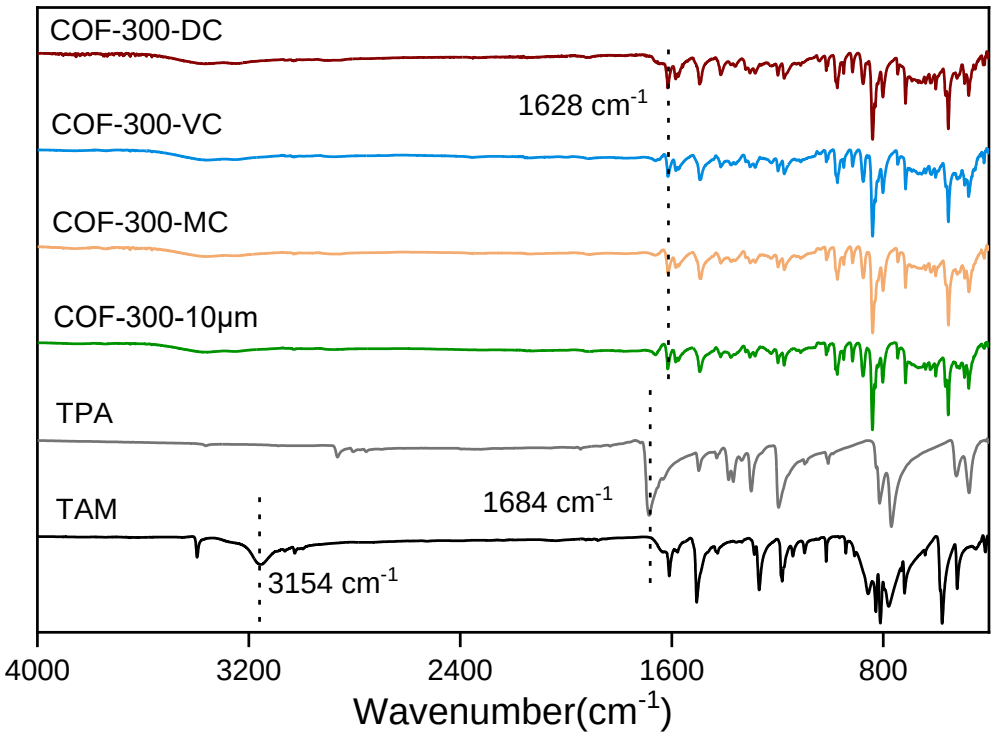

Figure S1. The FT-IR spectra of COF-300-MC (orange), -VC (blue), -DC (red), and -10μm(green). FT-IR spectra show that the characteristic peaks of TPA (grey) at 1684 cm^{-1} and TAM (black) at 3154 cm^{-1} disappeared. And the characteristic peaks of imine bond at 1628 cm^{-1} appear in COF-300-MC, -VC, -DC, and -10μm, indicating that the reaction of the organic linker is complete.

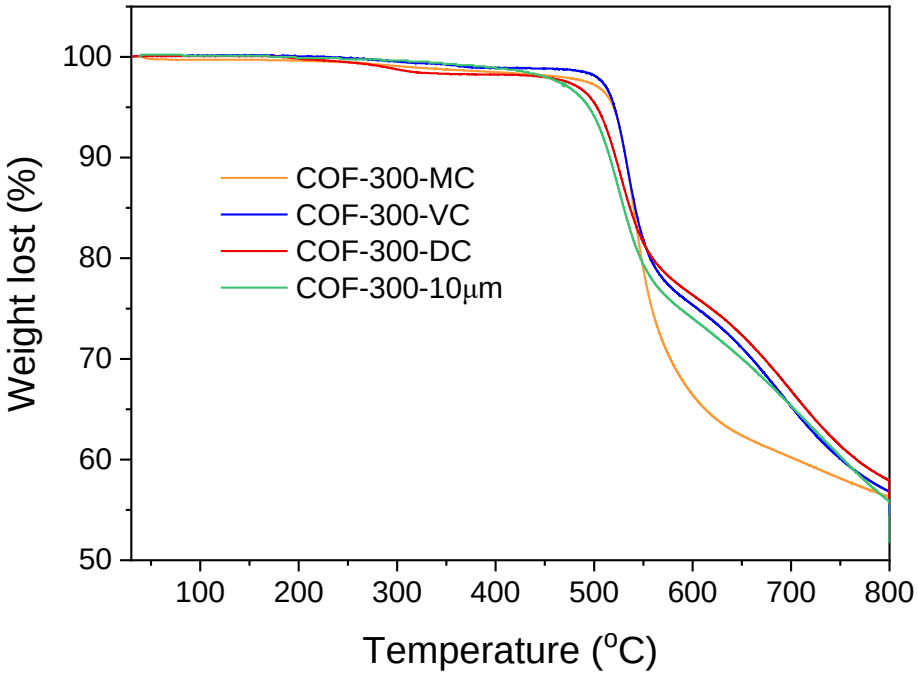

Figure S2. The TGA traces of COF-300-MC (orange), -VC (blue), -DC (red), and -10μm(green) to test the decomposition temperature of the sample at 30-800 °C at a rate of 5 °C per minute. The TGA curves of the tested samples were differentiated to determine the decomposition temperature. The decomposition temperatures of COF-300-MC, -VC, -DC, and -10μm were 538.8, 534.9, 525.9, and 528.8 °C, respectively.

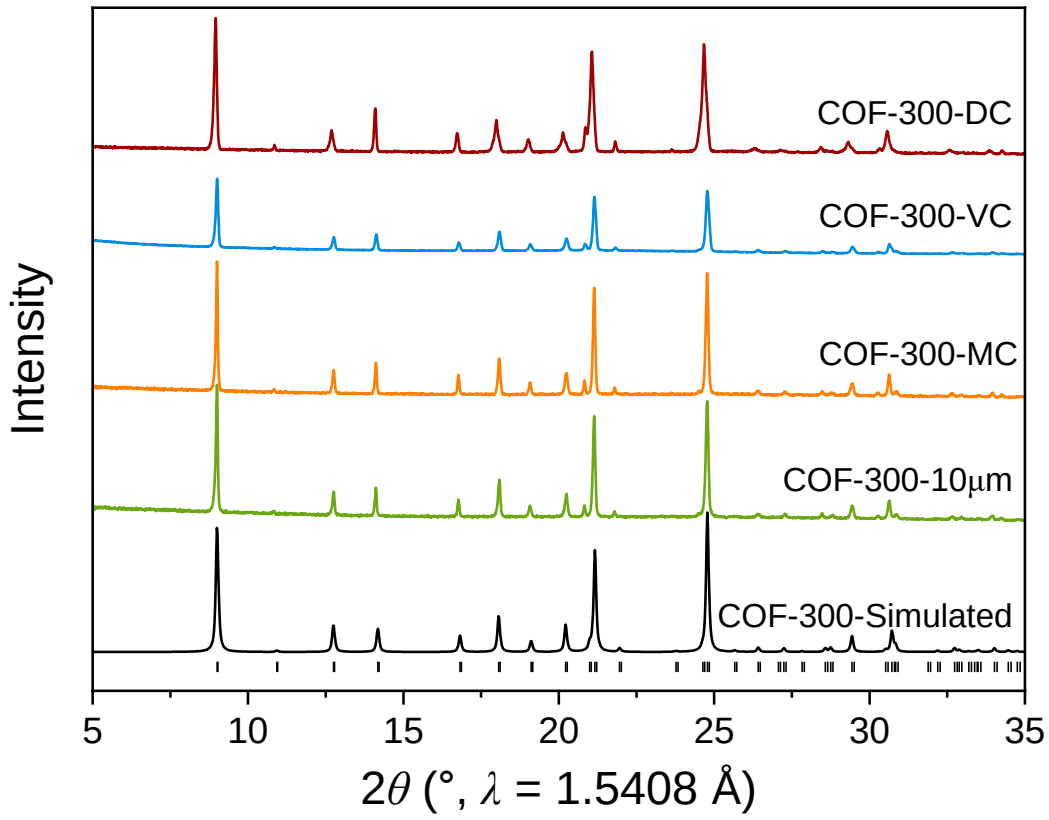

Figure S3. Comparison of PXRD patterns of the hydrated sample of COF-300-MC (orange), -VC (blue), and -DC (red) and -10 μm (green) with the simulated pattern (black). The full width at half maximum (FWHM)of 200 reflections of COF-300-MC (0.192°), -VC (0.094°), and -DC (0.123°) showing high crystallinity.

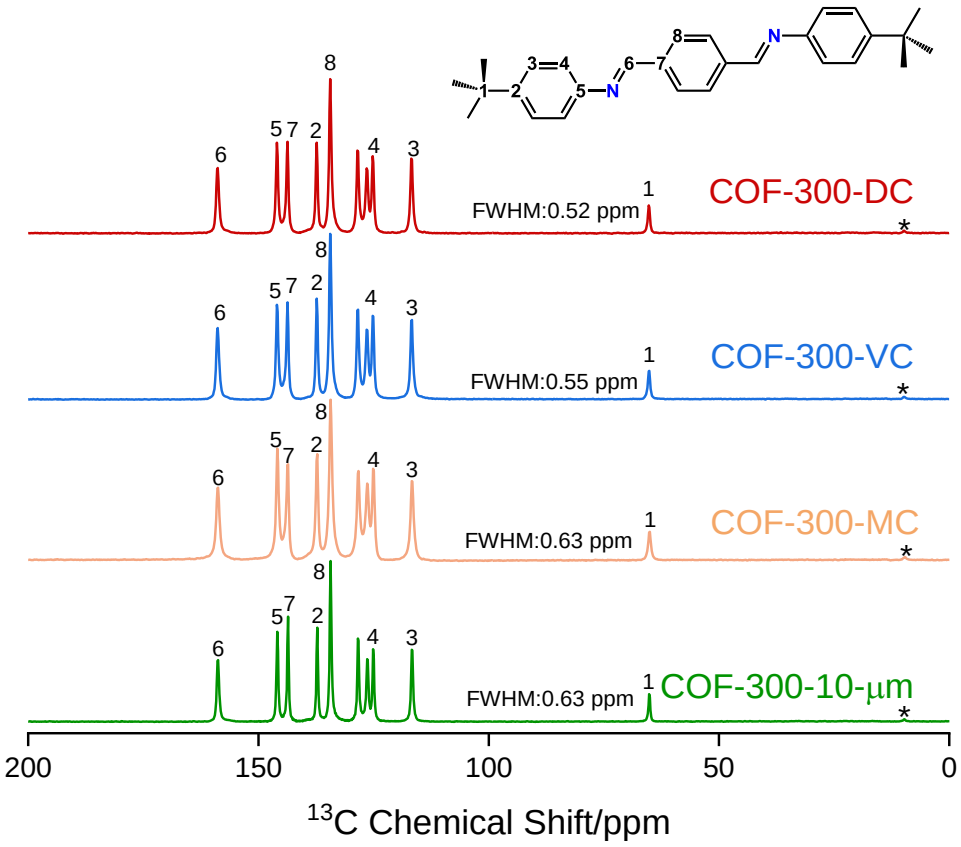

Figure S4. Comparison of solid-state CP/MAS ^{13}C NMR spectra of the hydrated COF-300-MC (orange), -VC (blue), -DC (red), and -10 μm (green) with narrow FWMH indicating the full conversion of raw materials and the high ordering of local chemical environments.

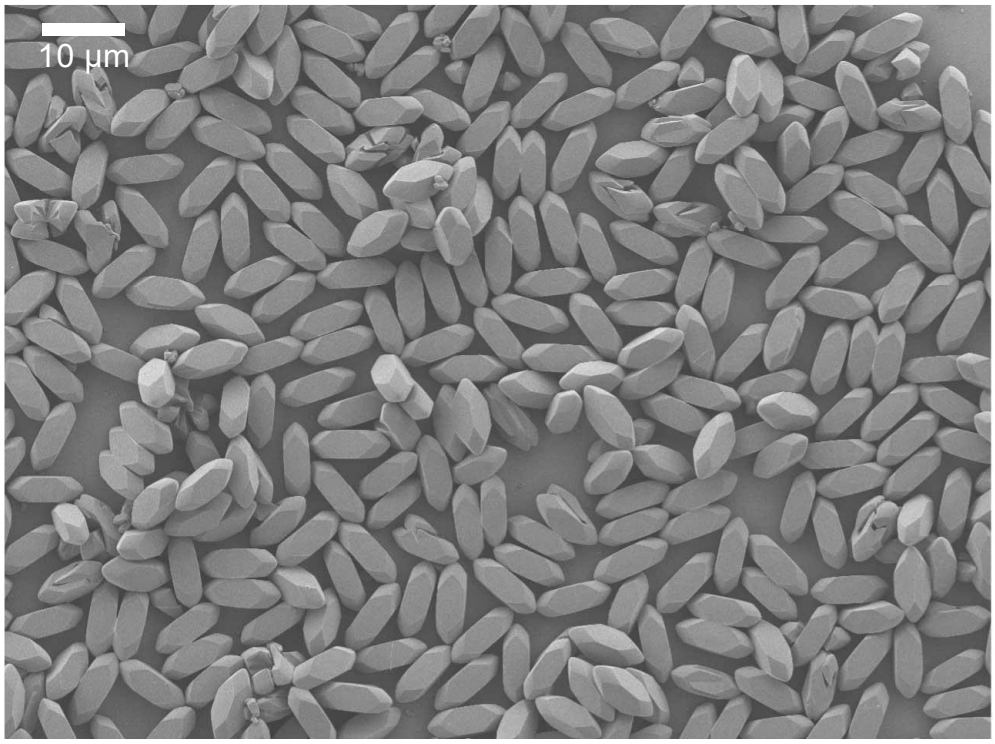

Figure S5. SEM image of COF-300-10 μm showing the well-defined crystal shapes and uniform crystal sizes.

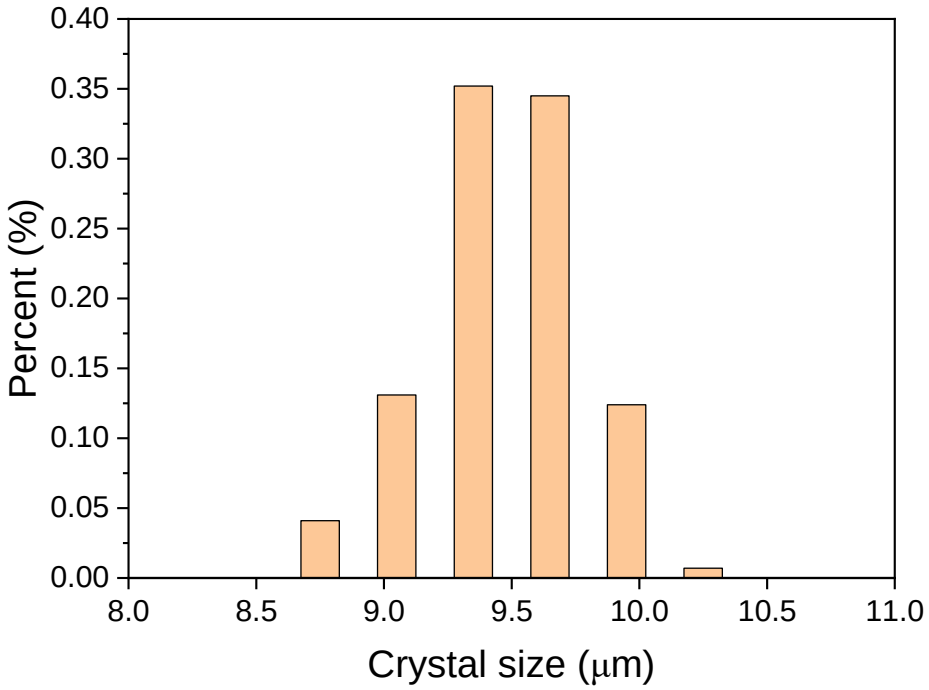

Figure S6. Histogram of crystal size distribution of COF-300-10 μm concentrated at 9.5 μm.

Section 2. Gas adsorption isotherms

Gas adsorption isotherms. The gas adsorption isotherms were collected using Autosorb IQ2 (Quantachrome) and BELSOP-MaxII adsorption apparatus, and Ultrahigh-purity CO_2 (>99.999%), N_2 (>99.999%), CH_4 (>99.999%), and *n*-Butane (>99.99%) in compressed gas cylinders were used through all experiments. Dewar with a mixture of sandy dry ice and MeOH was used to keep the sample temperatures at 195 K. Dewar with liquid nitrogen was used to keep the sample temperatures at 77 K and 112 K (with a cryocooler). Dewar connected to a Julabo F12-E0 isothermal bath filled with Ethylene glycol aqueous solution (v/v = 1:3), for which the temperature stability is ± 0.02 °C, was used to keep the temperature at 298 K.

To calculate the pore volume from saturated uptake, we use the equation as follow:

$$\boldsymbol{V}_{\mathrm{p}} = \frac{\boldsymbol{V_a m_g}}{\boldsymbol{V_m \rho_l}} \ ,$$

where V_{p} represents pore volume, V_a represents saturated uptake, V_m represents the molar volume of the gas, m_g represents the molar mass of the gas, and ρ_l represents the density of the guest matter in the liquid state.

To better demonstrate the host-guest relationship in COF-300 during adsorption, the measuring unit of gas uptake can be converted to mol/mol according to the following equation:

$$\boldsymbol{n_{ads}} = \frac{\boldsymbol{V_a m_{COF-300}}}{\boldsymbol{V_m}},$$

where n_{ads} represents the uptake after conversion, and $m_{\mathrm{COF\text{-}300}}$ represents the molar mass of COF-300.

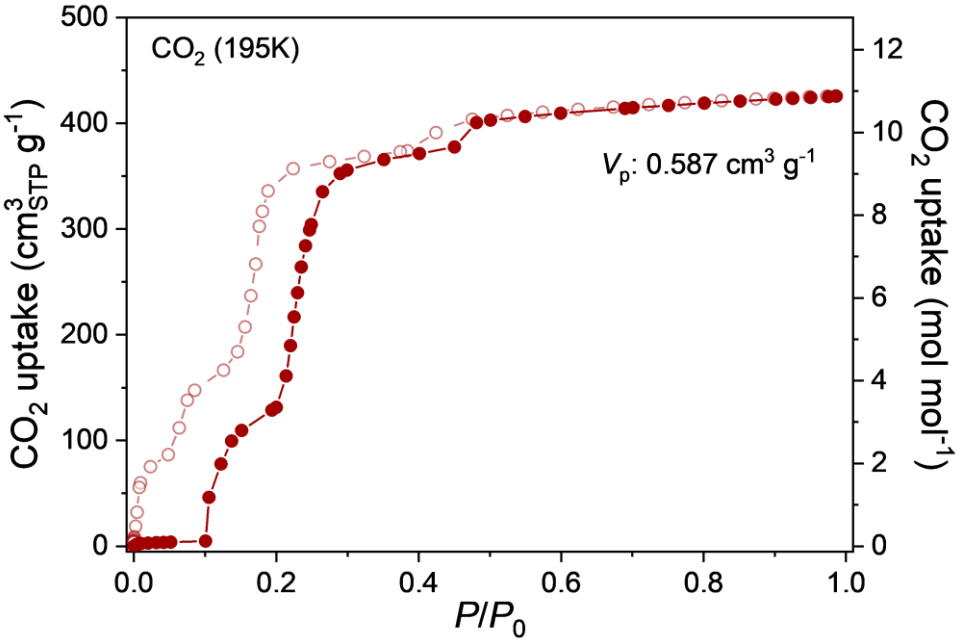

Figure S7. CO_2 adsorption isotherm at 195 K of COF-300-DC. The adsorption saturation is 11 mol/mol, and the corresponding V_p is 0.587 cm^3/g.

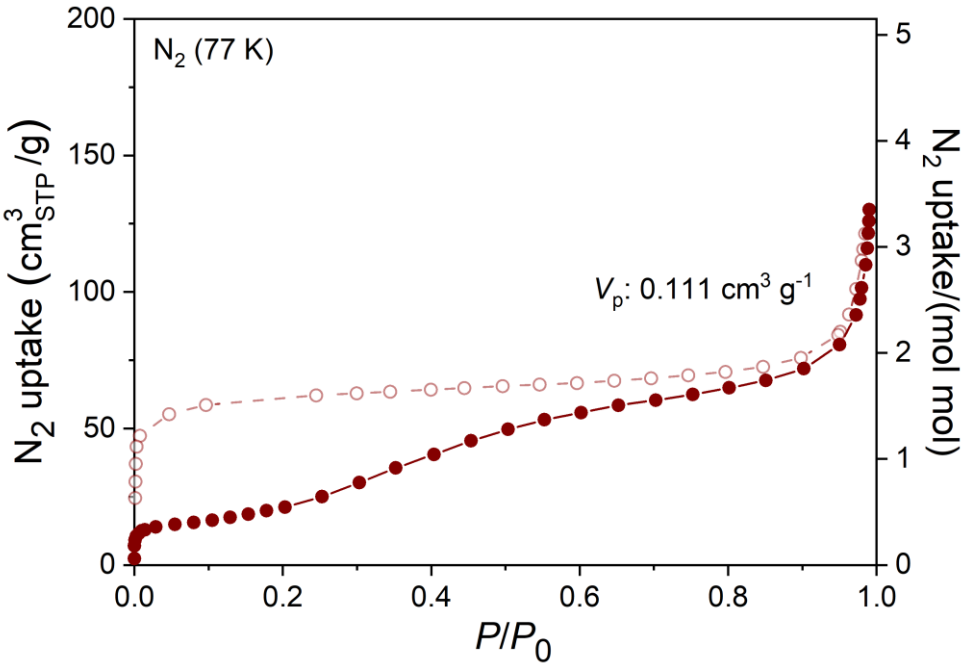

Figure S8. N_2 adsorption isotherm at 77 K of COF-300-DC. The adsorption saturation is ~2 mol/mol, and the corresponding V_p is 0.111 cm^3/g.

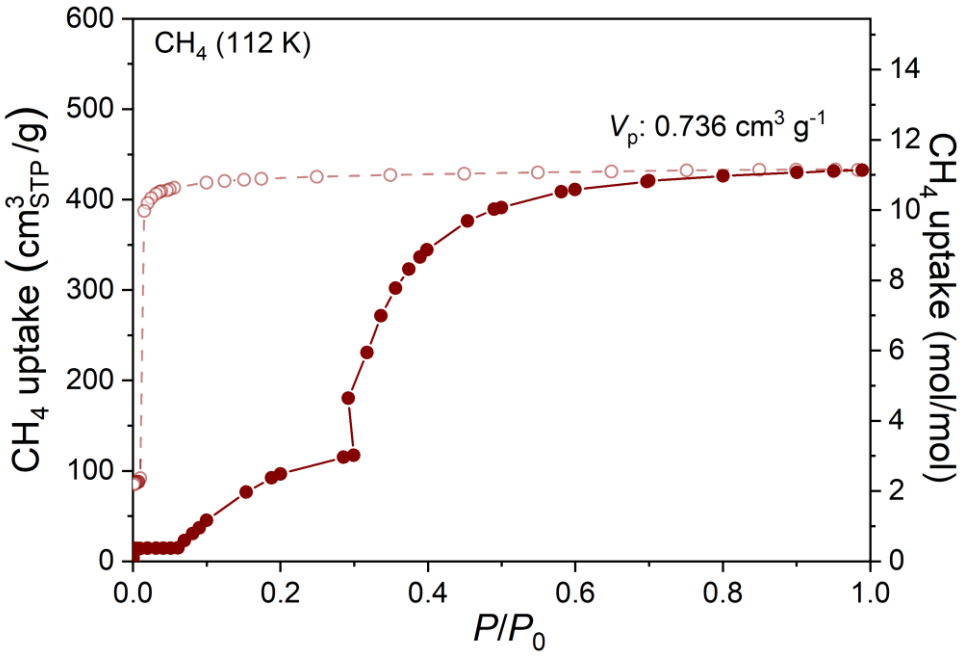

Figure S9. CH_4 adsorption isotherm at 112 K of COF-300-DC. The adsorption saturation is ~11 mol/mol, and the corresponding V_p is 0.736 cm^3/g.

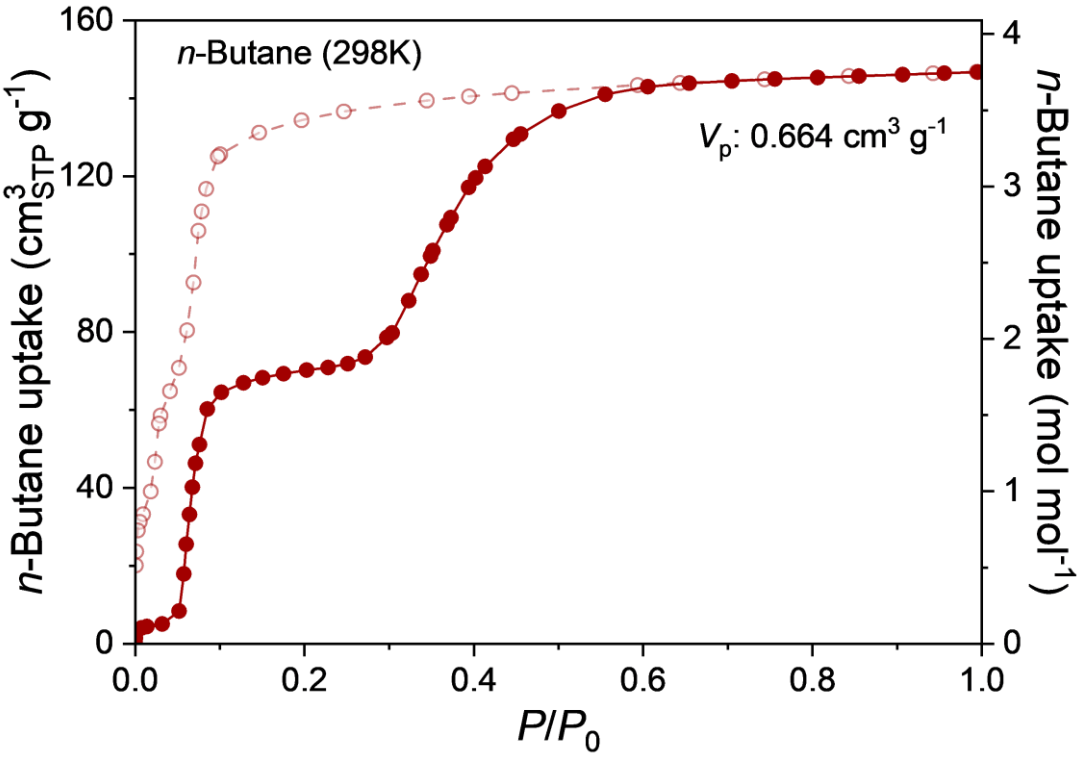

Figure S10. *n*-Butane adsorption isotherm at 298 K of COF-300-DC. The adsorption saturation is ~4 mol/mol, and the corresponding V_p is 0.664 cm^3/g.

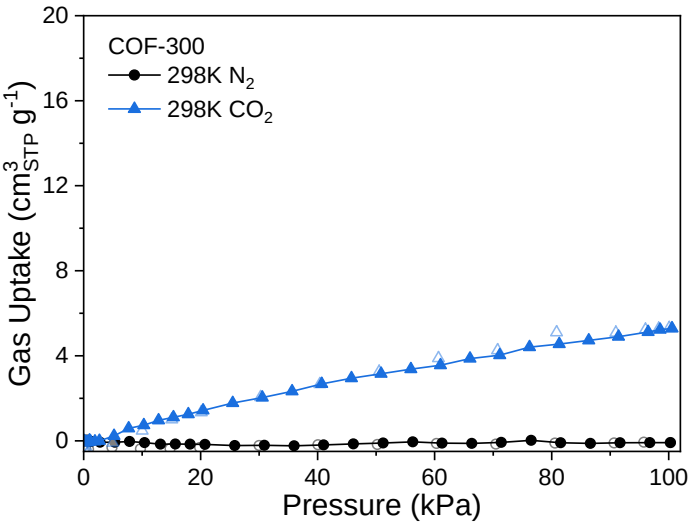

Figure S11. Comparison of gas adsorption isotherms of CO_2 and N_2 at 298 K for COF-300 with single crystal size of 50 μm.

Section 3. Organic vapor adsorption isotherms

Organic vapor adsorption isotherms. The organic vapor adsorption isotherms were collected using BELSORP-max and MicrotracBELSopr-Aqua3 adsorption apparatus with a water circulator bath. Coverage-dependent heats of organic vapor adsorption data was collected with an adsorption-calorimetric joint instrument constituted by MicrotracBEL Belsorp-MAXII and KEP ChemStar (ADS-CAL). Anhydrous solvents were used for vapor adsorption, which degassed at least five times before isotherm collection.

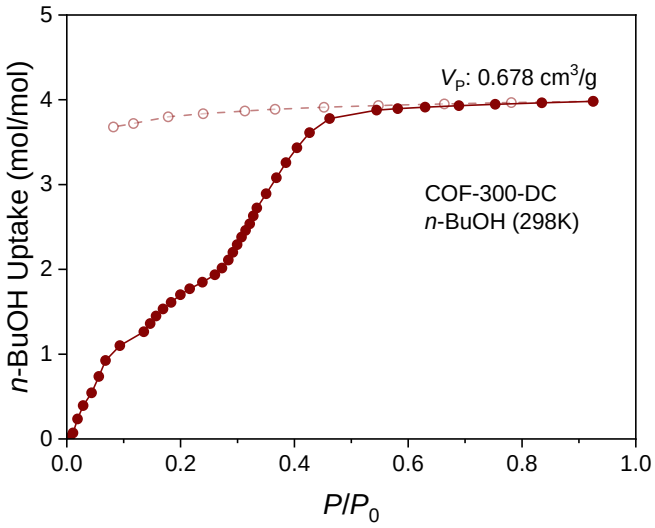

Figure S12. *n*-BuOH vapor adsorption isotherms at 298 K for COF-300-DC. The adsorption saturation is 4 mol/mol, and the corresponding V_p is 0.678 cm^3/g, which agrees with COF-300-op structure. The corresponding range of multi-step is P/P_0~0.56.

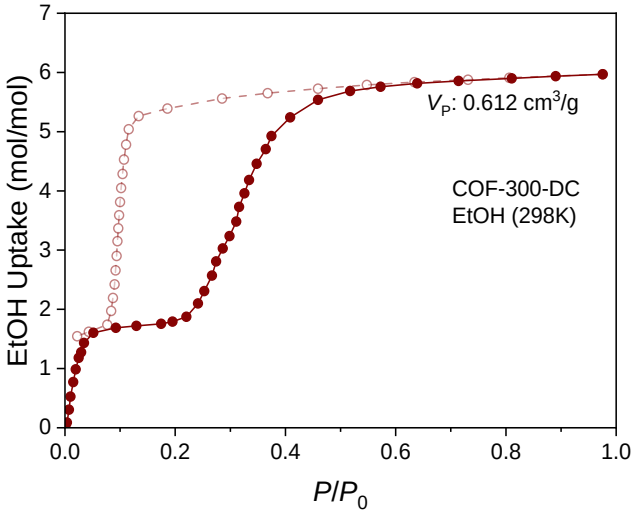

Figure S13. Ethanol vapor adsorption isotherms at 298 K for COF-300-DC. The adsorption saturation is 6 mol/mol, and the corresponding V_p is 0.612 cm^3/g, which agrees with COF-300-op structure. The corresponding range of multi-step is P/P_0~0.57.

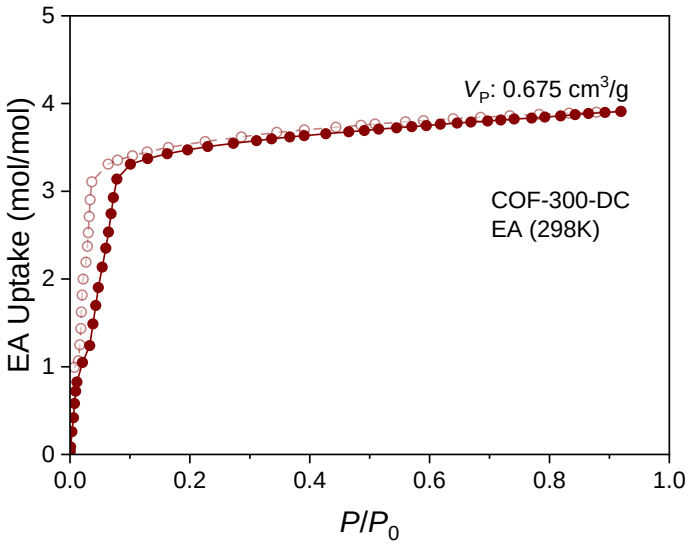

Figure S14. Ethyl Acetate (EA) adsorption isotherms at 298 K for COF-300-DC. The adsorption saturation is 4 mol/mol EA, and the corresponding V_p is 0.675 cm^3/g, which agrees with COF-300-op structure. The corresponding range of multi-step is P/P_0~0.13.

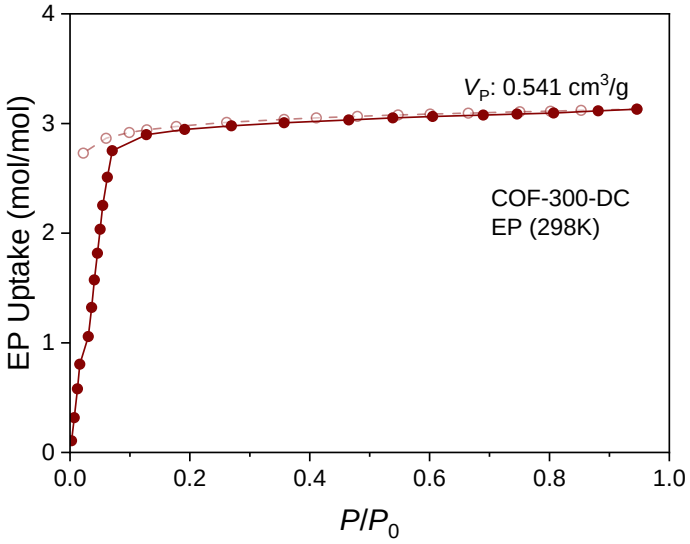

Figure S15. Ethyl Propanoate (EP) adsorption isotherms at 298 K for COF-300-DC. The adsorption saturation is 3 mol/mol EP, and the corresponding V_p is 0.541 cm^3/g, which agrees with COF-300-op structure. The corresponding range of multi-step is P/P_0~0.08.

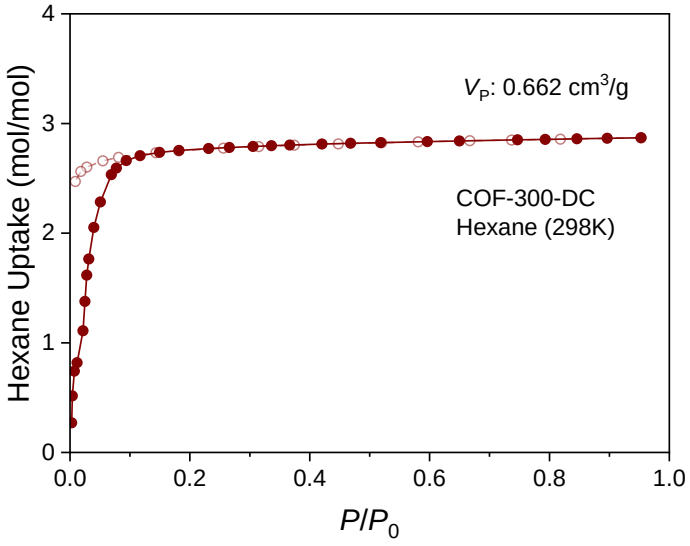

Figure S16. Hexane adsorption isotherms at 298 K for COF-300-DC. The adsorption saturation is 3 mol/mol hexane, and the corresponding V_p is 0.662 cm^3/g, which agrees with COF-300-op structure. The corresponding range of multi-step is P/P_0~0.09.

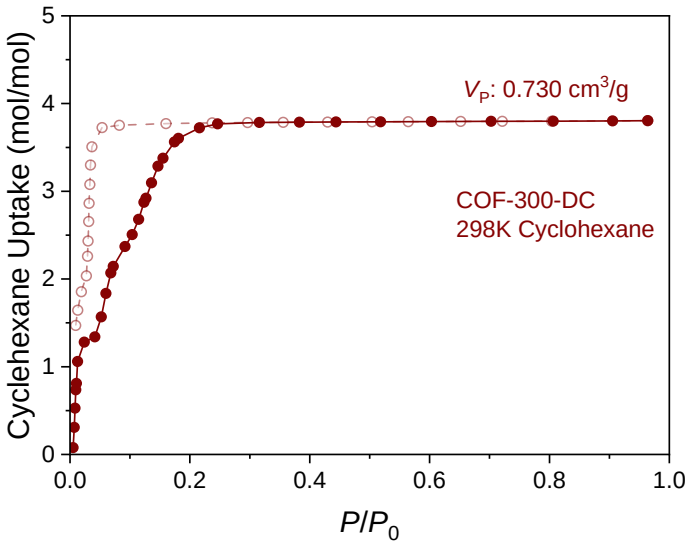

Figure S17. Cyclohexane adsorption isotherms at 298 K for COF-300-DC. The adsorption saturation is 4 mol/mol cyclohexane, and the corresponding V_p is 0.730 cm^3/g, which agrees with COF-300-op structure. The corresponding range of multi-step is P/P_0~0.25.

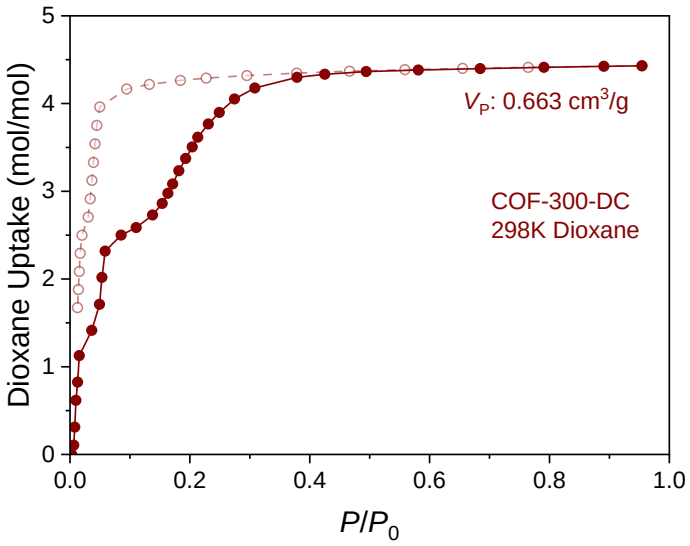

Figure S18. 1,4-Dioxane adsorption isotherms at 298 K for COF-300-DC. The adsorption saturation is 4 mol/mol dioxane, and the corresponding V_p is 0.663 cm^3/g, which agrees with COF-300-op structure. The corresponding range of multi-step is P/P_0~0.32.

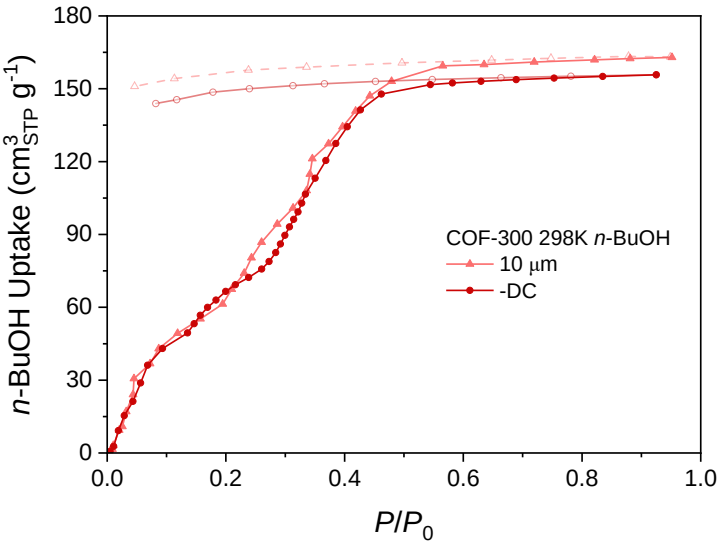

Figure S19. Comparison of vapour adsorption isotherms of *n*-BuOH at 298 K for COF-300 with single crystal size of 10 and 50 μm.

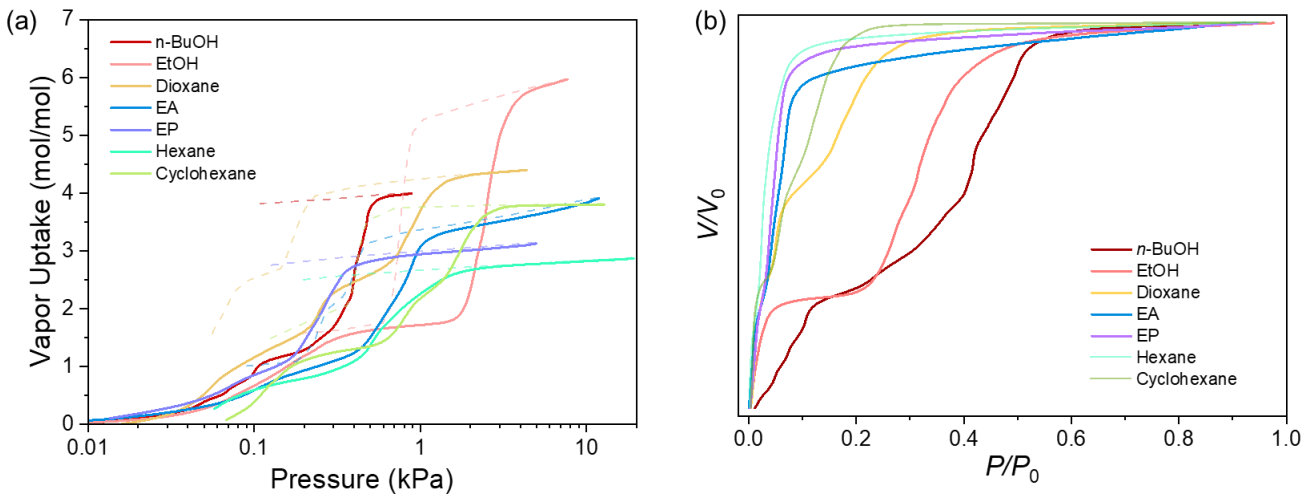

Figure S20. (a) Vapor uptakes of various organic solvents for COF-300 versus relative pressures, P/P_0, with normalized uptakes for comparing their adsorption isotherms. (b) Vapor uptakes of various organic solvents for COF-300 versus absolute pressures, P.

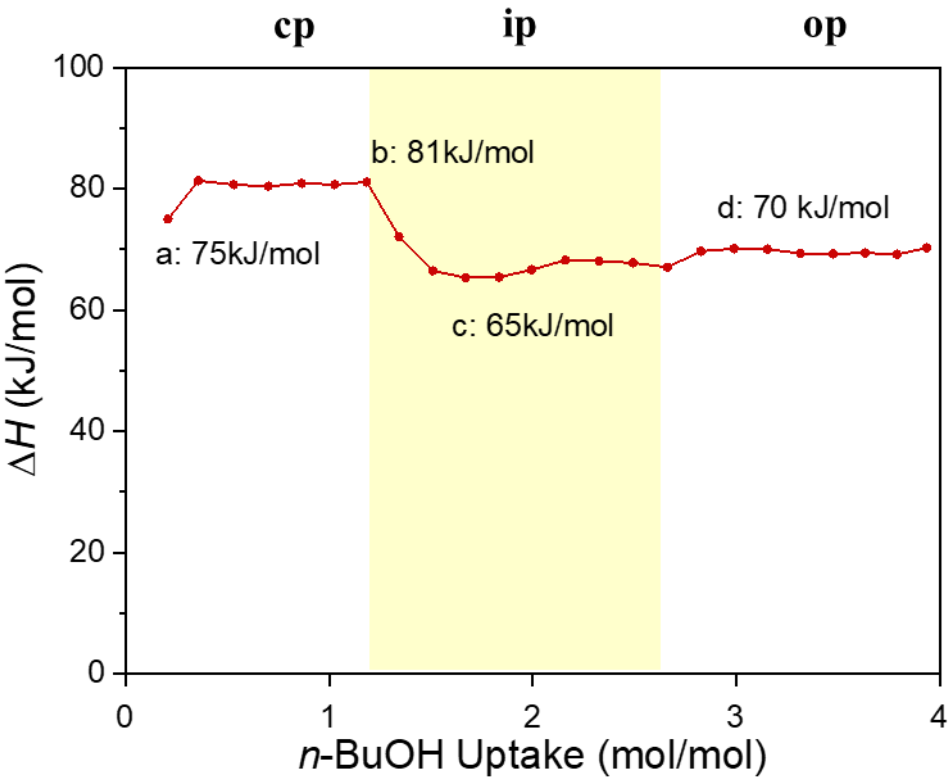

Figure S21. The microcalorimetry of COF-300 during *n*-BuOH adsorption indicating the endothermic effect of structural transformation fromCOF-300-cp to -ip.

Section 4. Single-crystal X-Ray crystallography

Single crystal X-ray diffraction data were collected at the Shanghai Synchrotron Light Source Line BL17B1/BL10U2 station and station equipped with a Dectris Pilatus3-2M/Dectris Eiger 16M, S/N E-32-0111 surface detector respectively. The structure was solved by direct methods using the SHELXTL[1] software package and further refined with different Fourier syntheses. All non-hydrogen atoms on the framework were refined anisotropically; all hydrogen atoms were generated geometrically and refined in the riding mode. All the phenyl rings were treated with rigid constraints.

Model precursor (MP). A needle-shaped crystal (80 × 10 × 10 μm^3) of hydrated COF-300-DC was measured at Bruker D8 venture.

Hydrated COF-300-DC. A prism-shaped crystal (60 × 20 × 10 μm^3) of hydrated COF-300-DC was measured at the SSRF. The single-crystal is evacuated to 55 mtorr on the Schlenk line for 24 hours and uses fumigation method to load H_2O.

Activated COF-300-DC. A prism-shaped crystal (60 × 20 × 10 μm^3) of COF-300-cp was measured at beamline BL10U2 at SSRF. The single-crystal was evacuated to 10 mtorr on the degassing station for 12 hours on 120 °C. After backfill with N_2, the sample were sealed in the glass capillary in a N_2 atmosphere glove box.

NBA@COF-300-ip. COF-300ip was prepared by N_2 purging of COF-300-op samples at room temperature for at least 90 minutes. A prism-shaped crystal (60 × 20 × 10 μm^3) of *n*-BuOH@COF-300-ip was measured at SSRF.

NBA@COF-300-op. COF-300-cp was fumigated for 6 hours at 40°C around NBA atmosphere. A prism-shaped crystal (60 × 20 × 10 μm^3) of COF-300op was measured at SSRF.

NPA@COF-300-ip. COF-300-ip was prepared by N_2 purging of COF-300-op samples at room temperature for at least 120 minutes. A prism-shaped crystal of NPA@COF-300-ip was measured at SSRF.

NPA@COF-300-op. COF-300-cp was fumigated for 6 hours at 40°C around NPA atmosphere. A prism-shaped crystal (60 × 20 × 10 μm^3) of COF-300op was measured at SSRF.

NHA@COF-300-ip. COF-300-ip was prepared by N_2 purging of COF-300-op samples at room temperature for at least 180 minutes. A prism-shaped crystal of NHA@COF-300-ip was measured at SSRF.

NHA@COF-300-op. COF-300-cp was fumigated for 6 hours at 40°C around NHA atmosphere. A prism-shaped crystal (60 × 20 × 10 μm^3) of COF-300-op was measured at SSRF.

MB@COF-300-op. COF-300-cp was fumigated for 6 hours at 40°C around MB atmosphere. A prism-shaped crystal (60 × 20 × 10 μm^3) of COF-300-op was measured at SSRF.

IAA@COF-300-op. COF-300-cp was fumigated for 6 hours at 40°C around IAA atmosphere. A prism-shaped crystal (60 × 20 × 10 μm^3) of COF-300-op was measured at SSRF.

SPA@COF-300-op. COF-300-cp was fumigated for 6 hours at 40°C around SPA atmosphere. A prism-shaped crystal (60 × 20 × 10 μm^3) of COF-300-op was measured at SSRF.

BA@COF-300-op. COF-300-cp was fumigated for 6 hours at 60°C around BA atmosphere. A prism-shaped crystal (60 × 20 × 10 μm^3) of COF-300-op was measured at SSRF.

EL@COF-300-op. COF-300-cp was fumigated for 6 hours at 40°C around EL atmosphere. A prism-shaped crystal (60 × 20 × 10 μm^3) of COF-300-op was measured at SSRF.

PO@COF-300-op. COF-300-cp was fumigated for 6 hours at 100°C around SPA atmosphere. A prism-shaped crystal (60 × 20 × 10 μm^3) of COF-300-op was measured at SSRF.

GA@COF-300-op. COF-300-cp was fumigated for 6 hours at 40°C around GA atmosphere. A prism-shaped crystal (60 × 20 × 10 μm^3) of COF-300-op was measured at SSRF.

MF@COF-300-op. COF-300-cp was fumigated for 6 hours at 40°C around MF atmosphere. A prism-shaped crystal (60 × 20 × 10 μm^3) of COF-300-op was measured at SSRF.

EG@COF-300-op. COF-300-cp was immersed for 6 hours at room temperature. A prism-shaped crystal (60 × 20 × 10 μm^3) of COF-300-op was measured at SSRF.

All disordered molecular orientations were modeled as overlapping positions using PART -1. The guest molecules were refined with DFIX and SADI constraints.

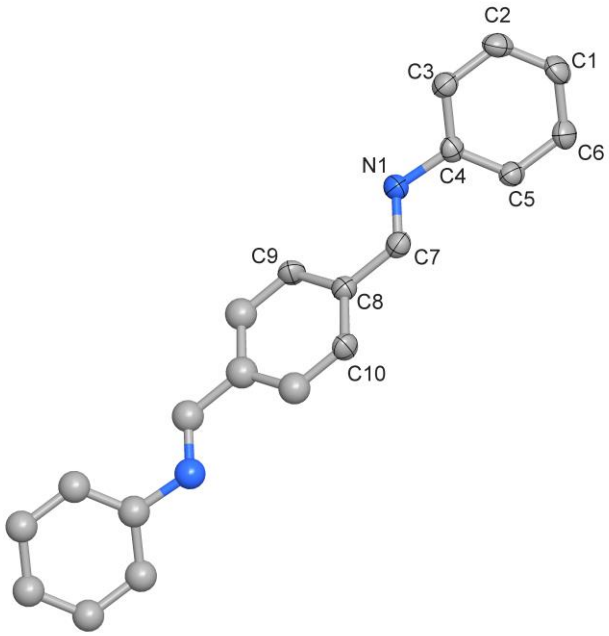

Figure S22. Thermal ellipsoid plot with 50% probability of the asymmetry unit for the single-crystal structure of MP (C, grey; N, blue). Hydrogen atoms are omitted for clarity; Symmetry-related atoms are not labelled and represented as spheres.

Table S1. Crystallography data and structure determination for MP

Compound	MP
Empirical formula	$C_{20}H_{16}N_2$
Formula weight	284.35
Crystal system	Monoclinic
Space group	$P2_1/c$ (15)
a (Å)	7.5587(16)
b (Å)	6.0473(11)
c (Å)	16.428(3)
α (º)	90
β (º)	91.114(11)
γ (º)	90
V (Å^3)	750.8(3)
Z	2
F(000)	300.0
Crystal density (g/cm^3)	1.258
Absorption coefficient (mm^{-1})	0.365
Crystal size (μm)	80x10x10
Temperature (K)	100
Radiation	GaKα
Wavelength (Å)	1.3418
2θ range for data collection	9.368/105.336
Index ranges	-8≤h≤8/-6≤k≤6/-18≤l≤16
Total/Unique data	6698/1238
R_{int} (%)	7.68
Observed data [I＞2σ(I)]	931
R_1[I＞2σ(I)][a]	0.0644
wR_2 (all data)[b]	0.1620
S[c]	1.081
Completeness (%)	94.6
Largest diff. peak/hole (e/Å^3)	0.24/-0.20
CCDC number	2401544

[a] $R_1 = \Sigma||F_o| - |F_c||/ \Sigma|F_o|$; [b] $wR_2 = [\Sigma w(F_o^2 - F_c^2)^2/\Sigma w(F_o^2)^2]^{1/2}$; [c] $S = [\Sigma w(F_o^2 - F_c^2)^2/(N_{ref} - N_{par})]^{1/2}$.

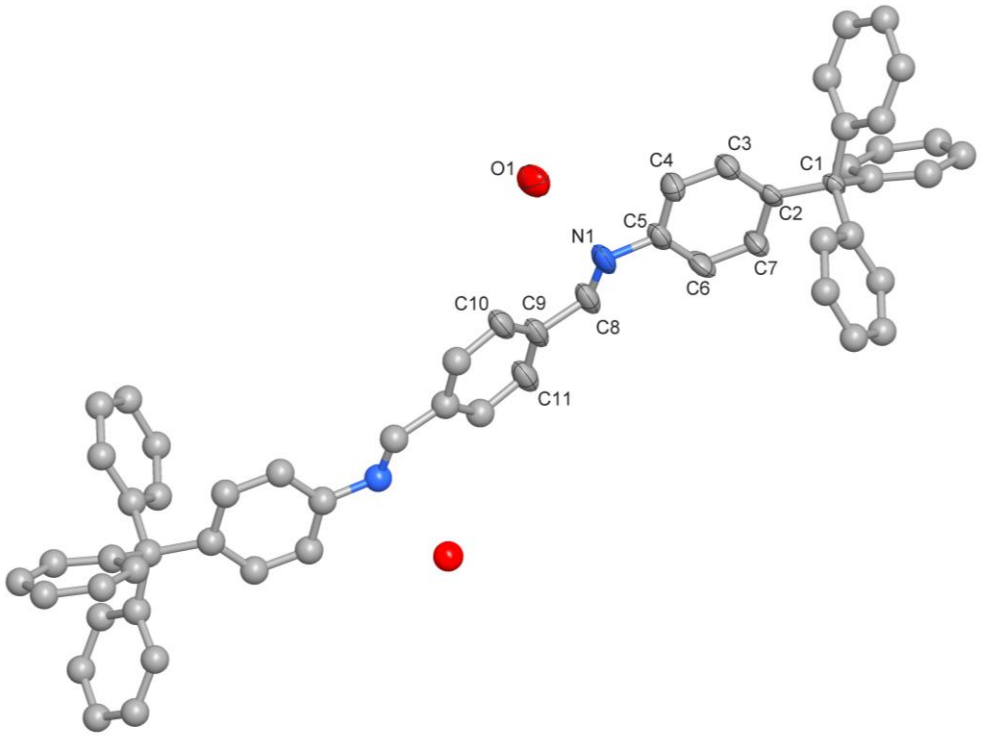

Figure S23. Thermal ellipsoid plot with 50% probability of the asymmetry unit for the single-crystal structure of hydrated COF-300-DC (C, grey; N, blue; O, red). Hydrogen atoms are omitted for clarity; Symmetry-related atoms are not labelled and represented as spheres.

Table S2. Crystallography data and structure determination for hydrated COF-300-DC

Compound	Hydrated COF-300-DC
Empirical formula	$C_{41}H_{28}N_4 \cdot 3.6H_2O$
Formula weight	641.53
Crystal system	Tetragonal
Space group	$I4_1/a$ (88)
a (Å)	19.5107(6)
b (Å)	19.5107(6)
c (Å)	8.9850(4)
α (º)	90
β (º)	90
γ (º)	90
V (Å^3)	3420.3(3)
Z	4
F(000)	1352.0
Crystal density (g/cm^3)	1.246
Absorption coefficient (mm^{-1})	0.081
Crystal size (μm)	60x20x10
Temperature (K)	100
Radiation	18 KeV
Wavelength (Å)	0.6888
2θ range for data collection	4.176/57.39
Index ranges	-24≤h≤24/-24≤k≤25/-9≤l≤10
Total/Unique data	18598/2083
R_{int} (%)	5.66
Observed data [I>2σ(I)]	1819
R_1[I>2σ(I)][a]	0.0541
wR_2 (all data)[b]	0.1485
S[c]	1.036
Completeness (%)	98.7
Largest diff. peak/hole (e/Å^3)	0.36/-0.21
CCDC number	2385497

[a] $R_1 = \Sigma||F_o| - |F_c||/ \Sigma|F_o|$; [b] $wR_2 = [\Sigma w(F_o^2 - F_c^2)^2/\Sigma w(F_o^2)^2]^{1/2}$; [c] $S = [\Sigma w(F_o^2 - F_c^2)^2/(N_{ref} - N_{par})]^{1/2}$.

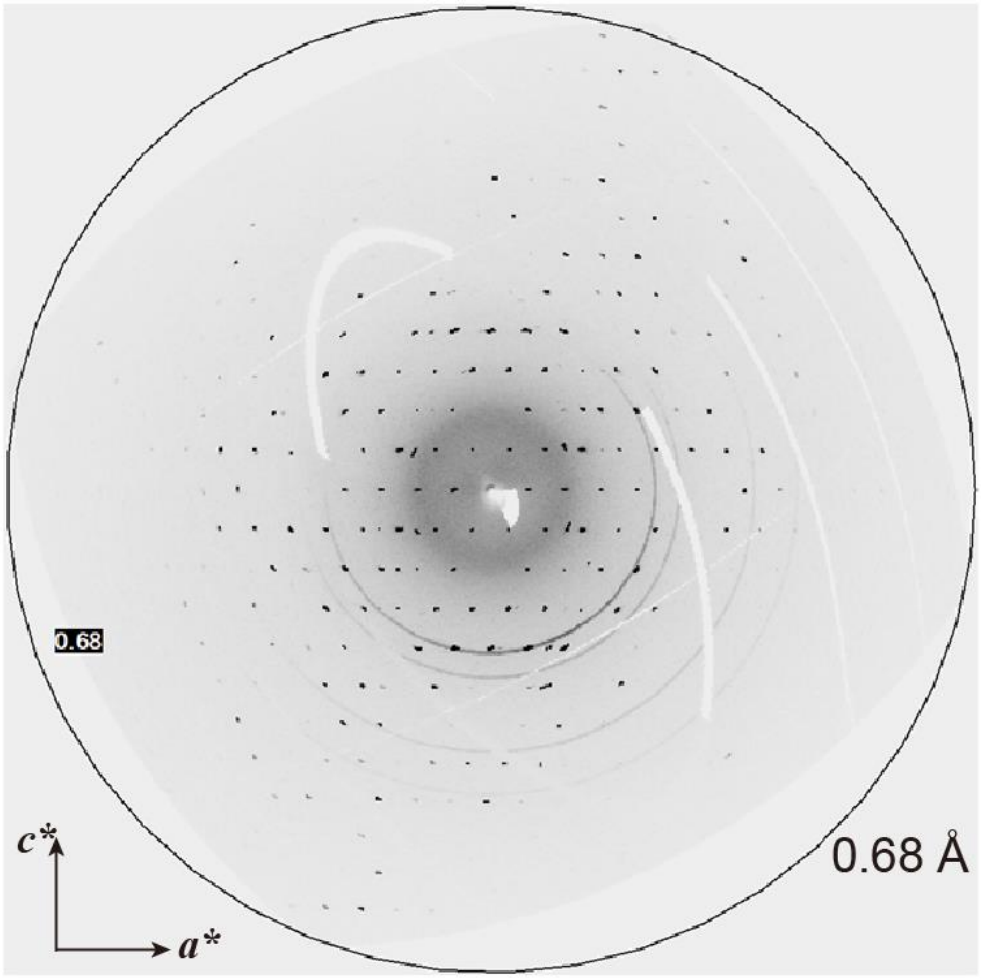

Figure S24. The (*h*0*l*) slice of the reconstructed single-crystal X-ray diffraction patterns of the hydrated COF-300-DC with a resolution better than 0.68 Å.

Table S3. Comparison of single-crystal X-ray diffraction data of COF-300 in completeness (%), resolution (Å), and R_{int} values.

	Completeness (%)	Resolution(Å)	R_{int}[d] (%)
COF-300-MC	96.4	<1 (0.91)	9.91
COF-300-VC	98.0	<1 (0.75)	10.81
COF-300-DC	98.7	<1 (0.74)	5.56

[d] $R_{int} = \Sigma|F_o^2 - F_o^2(\text{mean})| / \Sigma[(F_o^2)]$

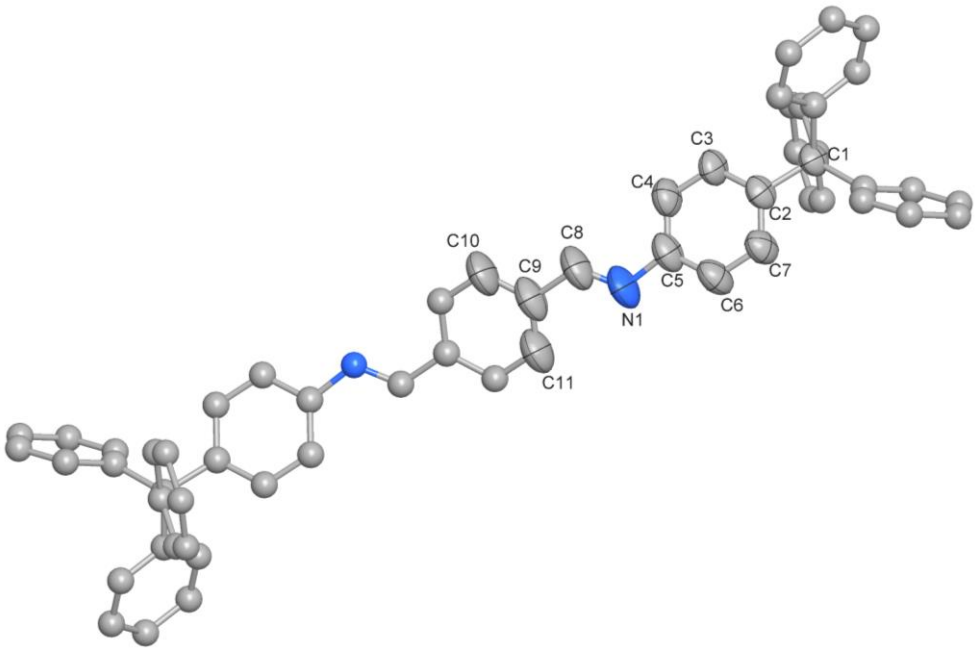

Figure S25. Thermal ellipsoid plot with 50% probability of the asymmetry unit for the single-crystal structure of COF-300-cp (C, grey; N, blue). Hydrogen atoms were omitted for clarity; symmetry-related atoms were not labelled and represented as spheres.

Table S4. Crystallography data and structure determination for COF-300-cp.

Compound	COF-300-cp
Cell formula	$C_{41}H_{28}N_4$
Formula weight	576.67
Crystal system	Tetragonal
Space group	$I4_1/a$ (88)
a (Å)	20.492(2)
b (Å)	20.492(2)
c (Å)	8.8184(13)
α (º)	90
β (º)	90
γ (º)	90
V (Å^3)	3703.0(9)
Z	4
F(000)	1208.0
Crystal density (g/cm^3)	1.034
Absorption coefficient (mm^{-1})	0.061
Crystal size (μm)	60x20x10
Temperature (K)	298.15
Radiation	18 KeV
Wavelength (Å)	0.6888
2θ range for data collection	2.81/43.87
Index ranges	-21≤h≤21/-20≤k≤19/-9≤l≤8
Total/Unique data	6680/1065
R_{int} (%)	5.66
Observed data [I＞2 σ(I)]	833
R_1[I＞2 σ(I)][a]	0.0582
wR_2 (all data)[b]	0.1320
S[c]	1.060
Completeness (%)	94.2
Largest diff. peak/hole (e/Å^3)	0.10/-0.10
CCDC number	2385499

[a] $R_1 = \Sigma||F_o| - |F_c||/\Sigma|F_o|$; [b] $wR_2 = [\Sigma w(F_o^2 - F_c^2)^2/\Sigma w(F_o^2)^2]^{1/2}$; [c] $S = [\Sigma w(F_o^2 - F_c^2)^2/(N_{ref} - N_{par})]^{1/2}$.

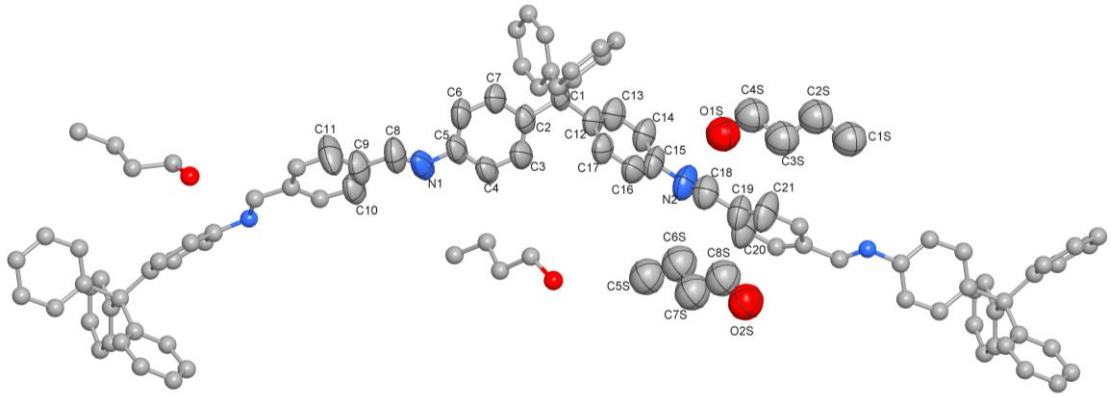

Figure S26. Thermal ellipsoid plot of the asymmetry unit for the single-crystal structure of NBA@COF-300-ip. (framework with 50% probability, NBA with 20% probability; C, grey; N, blue; O, red). Hydrogen atoms were omitted for clarity; symmetry-related atoms were not labelled and represented as spheres.

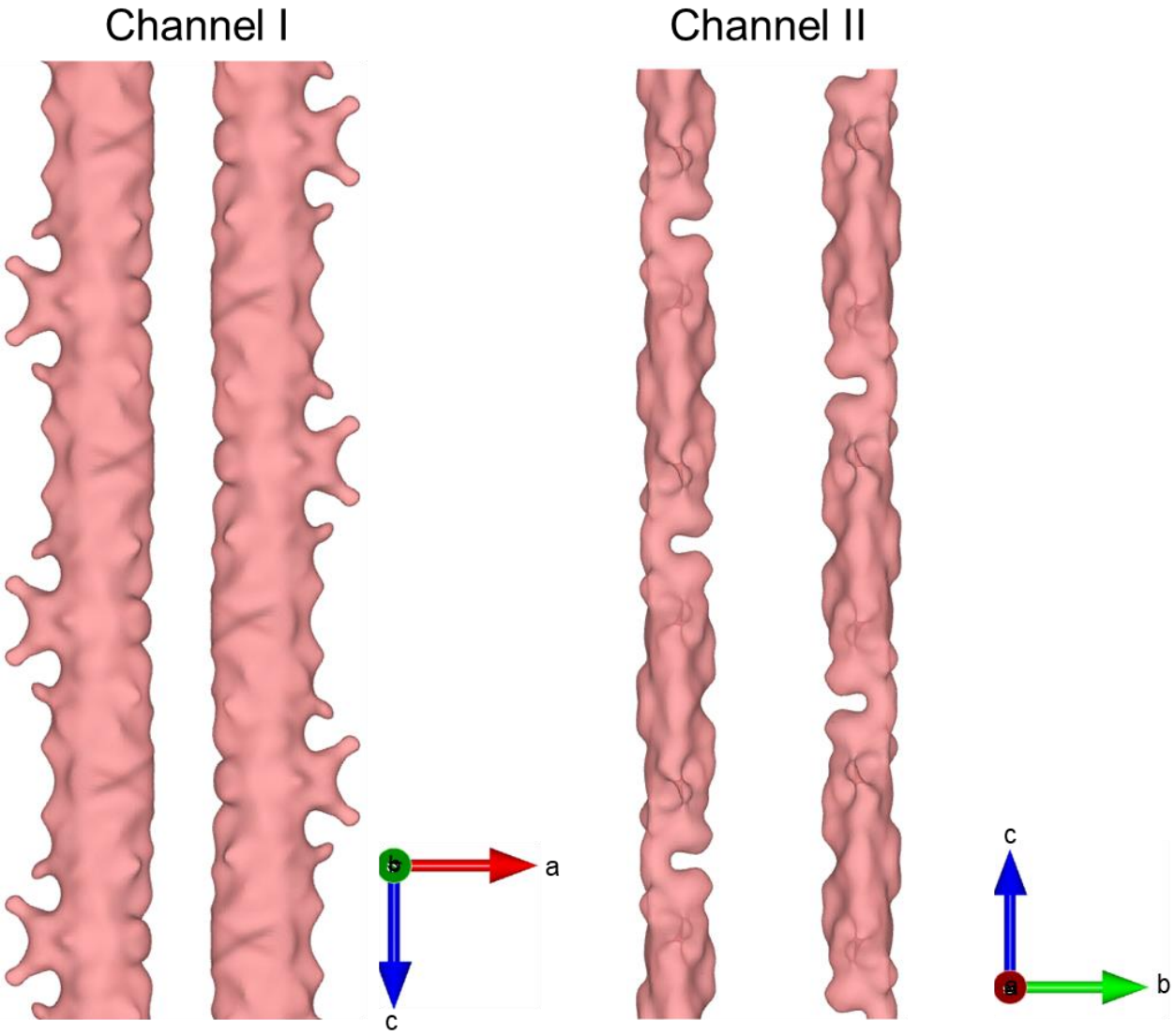

Figure S27. Color-coded 3D electron-density profile of NBA in COF-300-ip channel I (left) and channel II (right). Red isosurface level represents electron density of 0.263 eÅ^3.

Table S5. Crystallography data and structure determination for NBA@COF-300-ip

Compound	NBA@COF-300-ip
Cell formula	$C_{41}H_{28}N_4 \cdot 2C_4H_{10}O$
Formula weight	724.91
Crystal system	Orthorhombic
Space group	$I2_12_12_1(24)$
a (Å)	24.301(10)
b (Å)	20.762(8)
c (Å)	8.172(3)
α (º)	90
β (º)	90
γ (º)	90
V (Å^3)	4123(3)
Z	4
F(000)	1544.0
Crystal density (g/cm^3)	1.168
Absorption coefficient (mm^{-1})	0.071
Crystal size (μm)	60 x 20 x 10
Temperature (K)	RT
Wavelength (Å)	0.7106
2θ range for data collection	2.58/43.444
Index ranges	-25≤h≤23/-21≤k≤20/-8≤l≤8
Total/Unique data	5543/2151
R_{int} (%)	5.49
Observed data [I＞2 σ(I)]	1259
R_1[I＞2 σ(I)][a]	0.0878
wR_2 (all data)[b]	0.2681
S[c]	0.943
Completeness (%)	89.8
Largest diff. peak/hole (e/Å^3)	0.18/-0.17
CCDC number	2385500

[a] $R_1 = \Sigma||F_o| - |F_c||/\Sigma|F_o|$; [b] $wR_2 = [\Sigma w(F_o^2 - F_c^2)^2/\Sigma w(F_o^2)^2]^{1/2}$; [c] $S = [\Sigma w(F_o^2 - F_c^2)^2/(N_{ref} - N_{par})]^{1/2}$.

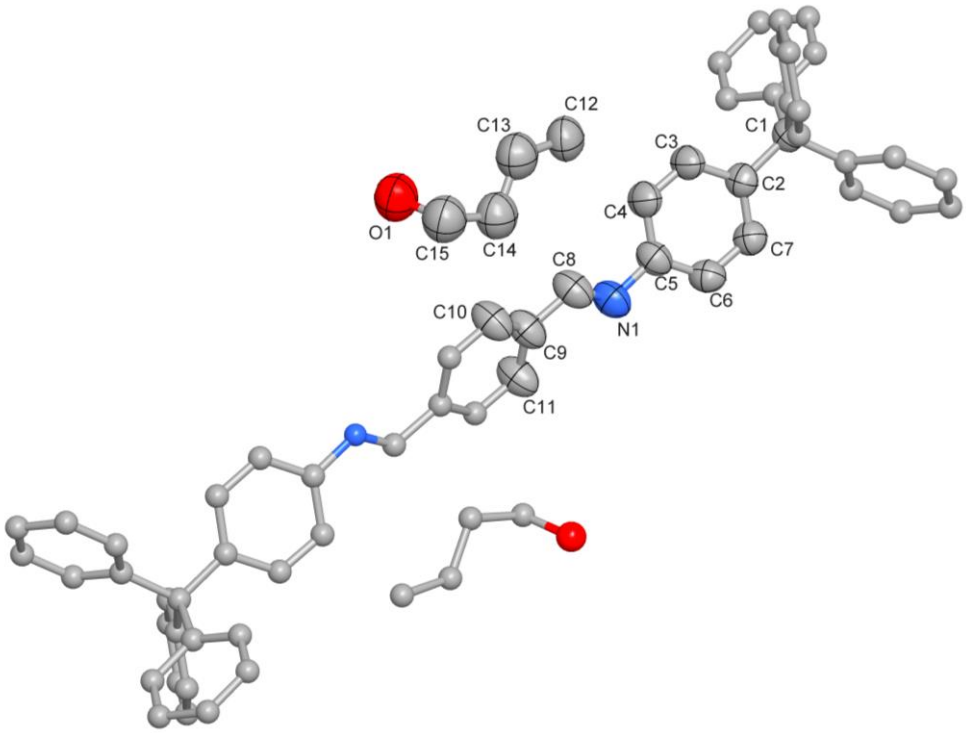

Figure S28. Thermal ellipsoid plot of the asymmetry unit for the single-crystal structure of NBA@COF-300-op (Framework with 50% probability, NBA with 20% probability; C, grey; N, blue; O, red). Hydrogen atoms were omitted for clarity; symmetry-related atoms were not labelled and represented as spheres.

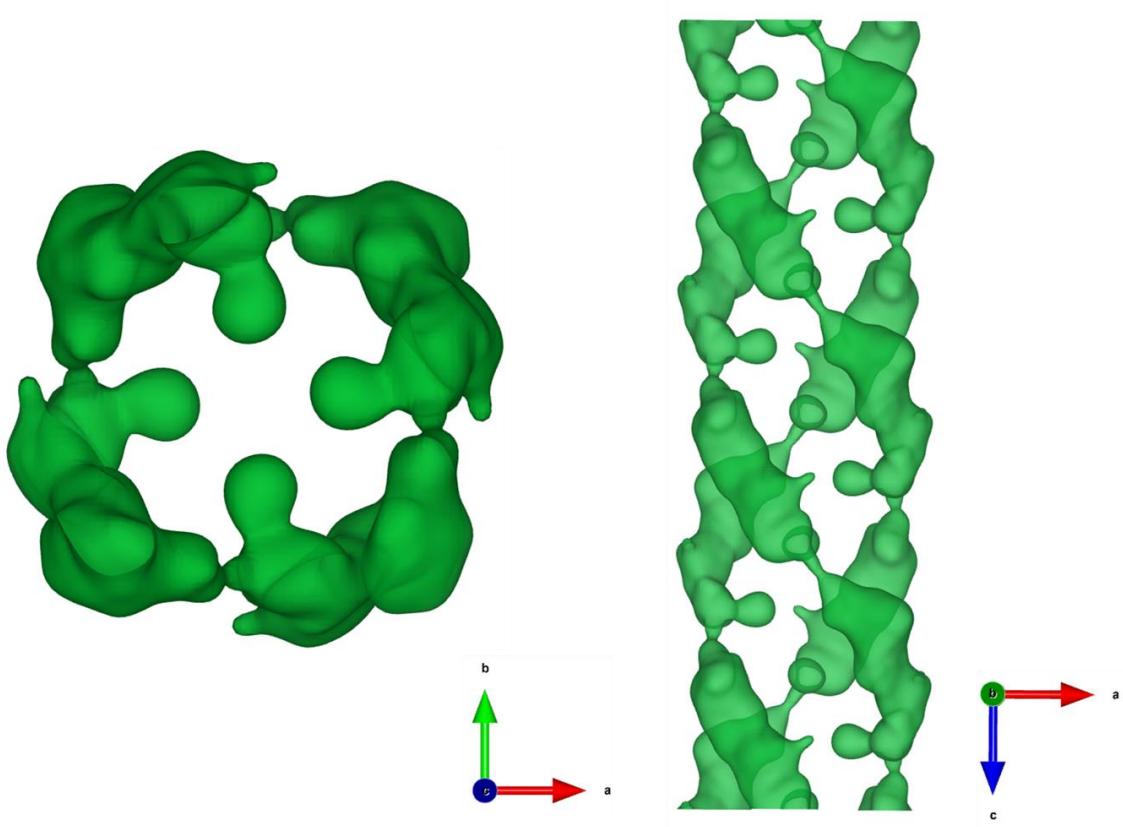

Figure S29. Color-coded 3D electron-density profile of NBA in COF-300-op *c*-axis (left) and *b*-axis (right). Green isosurface level represents electron density of 0.35 eÅ^3.

Table S6. Crystallography data and structure determination for NBA@COF-300-op

Compound	NBA@COF-300-op
Cell formula	$C_{41}H_{28}N_4 \cdot 4C_4H_{10}O$
Formula weight	873.15
Crystal system	Tetragonal
Space group	$I4_1/a$ (88)
a (Å)	25.4066(13)
b (Å)	25.4066(13)
c (Å)	7.7794(6)
α (°)	90
β (°)	90
γ (°)	90
V (Å^3)	5021.6(6)
Z	4
F(000)	1208.0
Crystal density (g/cm^3)	0.763
Absorption coefficient (mm^{-1})	0.045
Crystal size (μm)	60 x 20 x 10
Temperature (K)	100
Wavelength (Å)	0.6888
2θ range for data collection	6.414/52.72
Index ranges	-31≤h≤31/-31≤k≤31/-9≤l≤9
Total/Unique data	13784/2483
R_{int} (%)	3.54
Observed data [I＞2 σ(I)]	1972
R_1[I＞2 σ(I)][a]	0.1284
wR_2 (all data)[b]	0.3072
S[c]	1.063
Completeness (%)	97.0
Largest diff. peak/hole (e/Å^3)	0.32/-0.51
CCDC number	2385501

[a] $R_1 = \Sigma||F_o| - |F_c||/\Sigma|F_o|$; [b] $wR_2 = [\Sigma w(F_o^2 - F_c^2)^2/\Sigma w(F_o^2)^2]^{1/2}$; [c] $S = [\Sigma w(F_o^2 - F_c^2)^2/(N_{ref} - N_{par})]^{1/2}$.

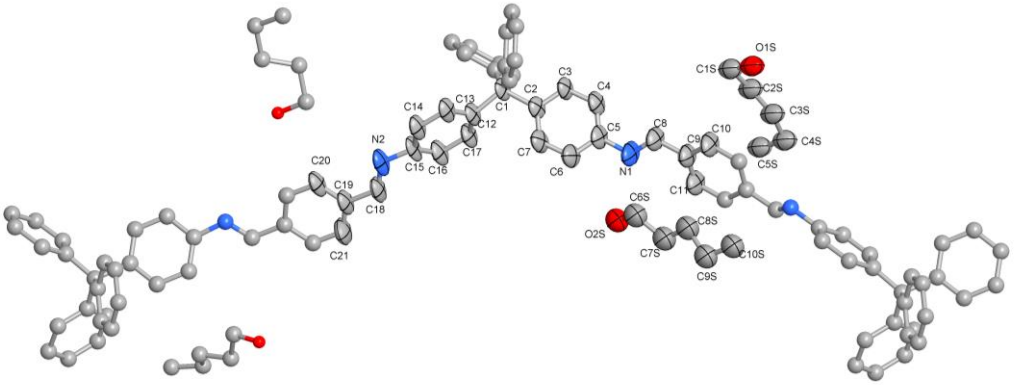

Figure S30. Thermal ellipsoid plot of the asymmetry unit for the single-crystal structure of NPA@COF-300-ip (Framework with 50% probability, NPA with 20% probability; C, grey; N, blue; O, red). Hydrogen atoms were omitted for clarity; symmetry-related atoms were not labelled and represented as spheres.

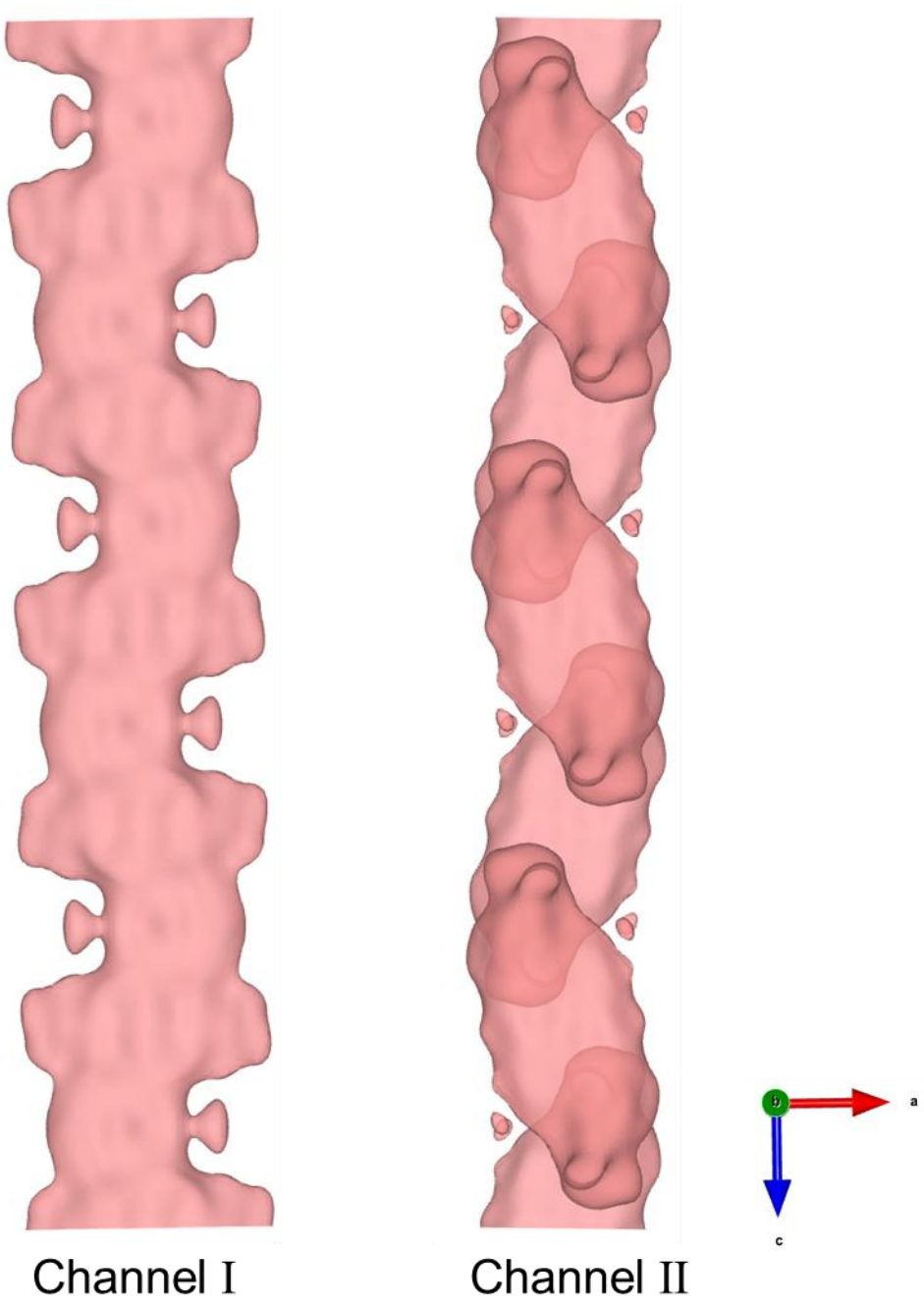

Figure S31. Color-coded 3D electron-density profile of NPA in COF-300-ip channel I (left) and channel II (right) in *b*-axis. Red isosurface level represents electron density of 0.467 eÅ^3.

Table S7. Crystallography data and structure determination for NPA@COF-300-ip

Compound	NPA@COF-300-ip
Cell formula	$C_{41}H_{28}N_4 \cdot 1.5C_5H_{12}O$
Formula weight	708.89
Crystal system	Orthorhombic
Space group	$I2_12_12_1(24)$
a (Å)	24.177(6)
b (Å)	20.366(5)
c (Å)	8.3463(17)
α (º)	90
β (º)	90
γ (º)	90
V (Å^3)	4109.5(16)
Z	4
F(000)	1508.0
Crystal density (g/cm^3)	1.146
Absorption coefficient (mm^{-1})	0.069
Crystal size (μm)	60 x 20 x 10
Temperature (K)	100
Wavelength (Å)	0.7107
2θ range for data collection	4.00/45.478
Index ranges	-26≤h≤23/-22≤k≤19/-8≤l≤8
Total/Unique data	7530/2583
R_{int} (%)	3.66
Observed data [I＞2σ(I)]	2076
R_1[I＞2σ(I)][a]	0.0771
wR_2 (all data)[b]	0.2330
S[c]	0.993
Completeness (%)	94.7
Largest diff. peak/hole (e/Å^3)	0.28/-0.19
CCDC number	2392142

[a]$R_1 = \Sigma||F_o| - |F_c||/\Sigma|F_o|$; [b]$wR_2 = [\Sigma w(F_o^2 - F_c^2)^2/\Sigma w(F_o^2)^2]^{1/2}$; [c]$S = [\Sigma w(F_o^2 - F_c^2)^2/(N_{ref} - N_{par})]^{1/2}$.

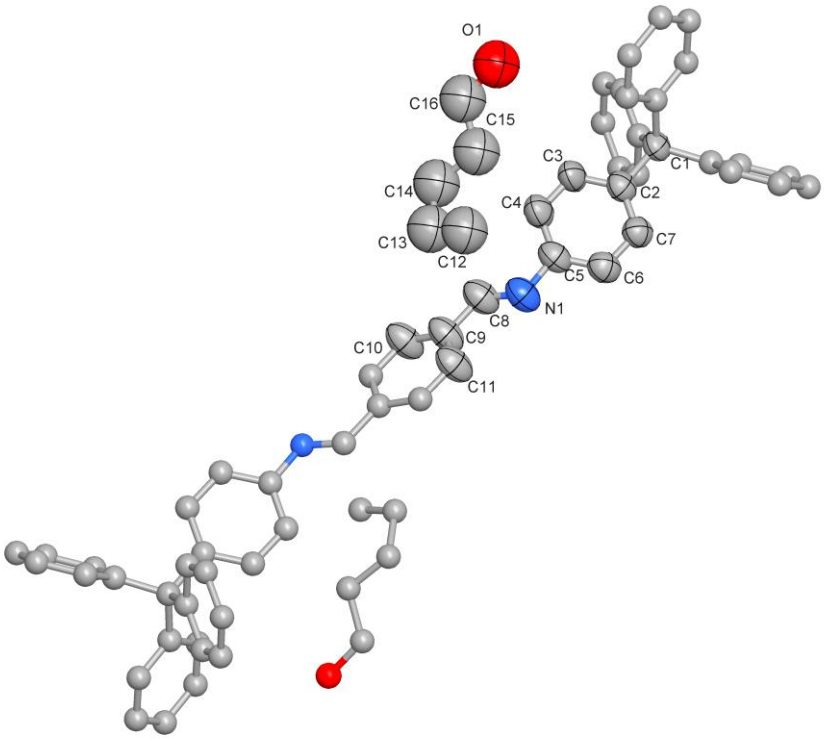

Figure S32. Thermal ellipsoid plot of the asymmetry unit for the single-crystal structure of NPA@COF-300-op (Framework with 50% probability, NPA with 20% probability; C, grey; N, blue; O, red). Hydrogen atoms were omitted for clarity; symmetry-related atoms were not labelled and represented as spheres.

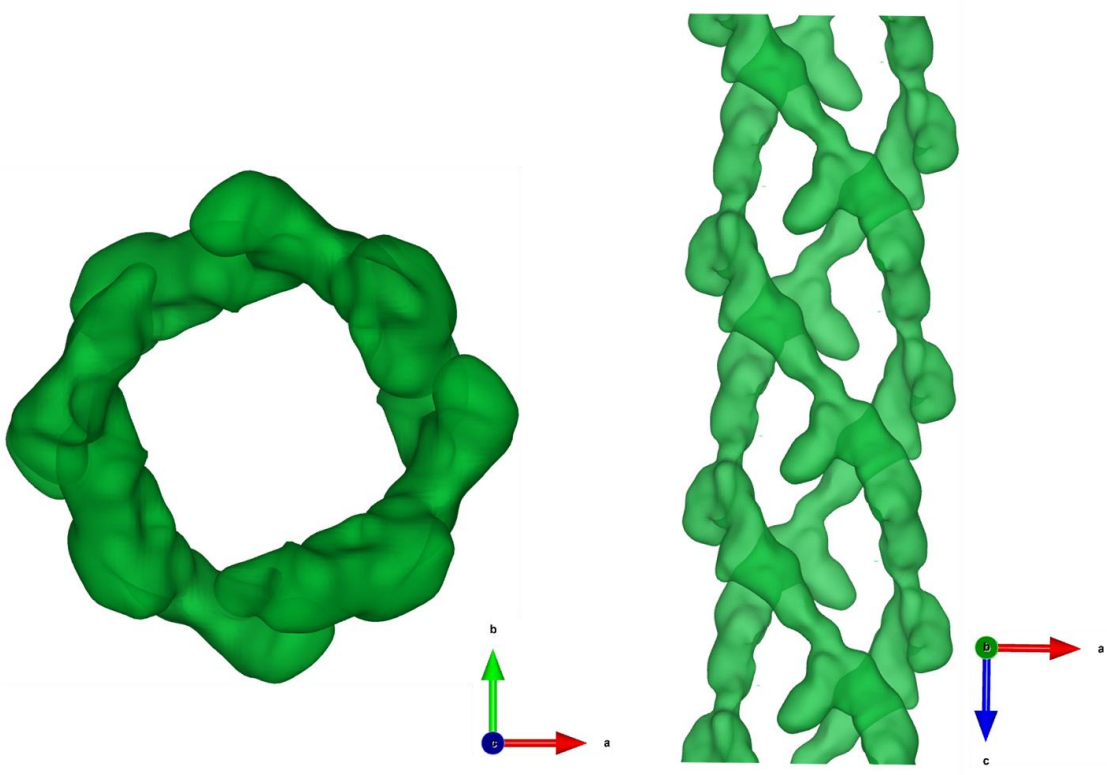

Figure S33. Color-coded 3D electron-density profile of NPA in COF-300-op *c*-axis (left) and *b*-axis (right). Green isosurface level represents electron density of 0.374 eÅ^3.

Table S8. Crystallography data and structure determination for NPA@COF-300-op

Compound	NPA@COF-300-op
Cell formula	$C_{41}H_{28}N_4 \cdot 3C_5H_{12}O$
Formula weight	841.44
Crystal system	Tetragonal
Space group	$I4_1/a$ (88)
a (Å)	25.3950(11)
b (Å)	25.3950(11)
c (Å)	7.7964(5)
α (º)	90
β (º)	90
γ (º)	90
V (Å^3)	5027.9(5)
Z	4
F(000)	1808.0
Crystal density (g/cm^3)	1.111
Absorption coefficient (mm^{-1})	0.068
Crystal size (μm)	60 x 20 x 10
Temperature (K)	100
Wavelength (Å)	0.7107
2θ range for data collection	5.466/49.424
Index ranges	-29≤h≤29/-29≤k≤29/-9≤l≤9
Total/Unique data	12224/2074
R_{int} (%)	3.48
Observed data [I＞2σ(I)]	1641
R_1[I＞2σ(I)][a]	0.1036
wR_2 (all data)[b]	0.2811
S[c]	1.056
Completeness (%)	96.5
Largest diff. peak/hole (e/Å^3)	0.34/-0.17
CCDC number	2385503

[a] $R_1 = \Sigma||F_o| - |F_c||/\Sigma|F_o|$; [b] $wR_2 = [\Sigma w(F_o^2 - F_c^2)^2/\Sigma w(F_o^2)^2]^{1/2}$; [c] $S = [\Sigma w(F_o^2 - F_c^2)^2/(N_{ref} - N_{par})]^{1/2}$.

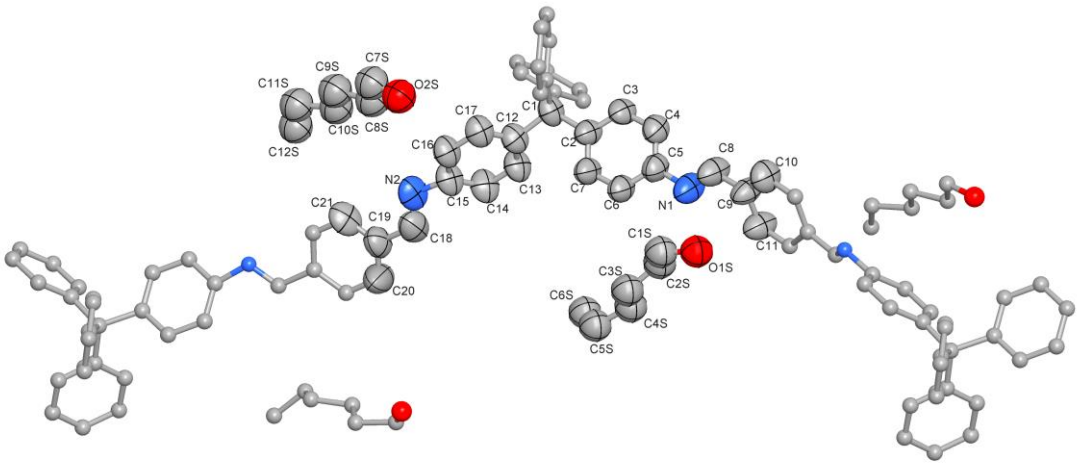

Figure S34. Thermal ellipsoid plot of the asymmetry unit for the single-crystal structure of NHA@COF-300-ip (Framework with 50% probability, NHA with 25% probability; C, grey; N, blue; O, red). Hydrogen atoms were omitted for clarity; symmetry-related atoms were not labelled and represented as spheres.

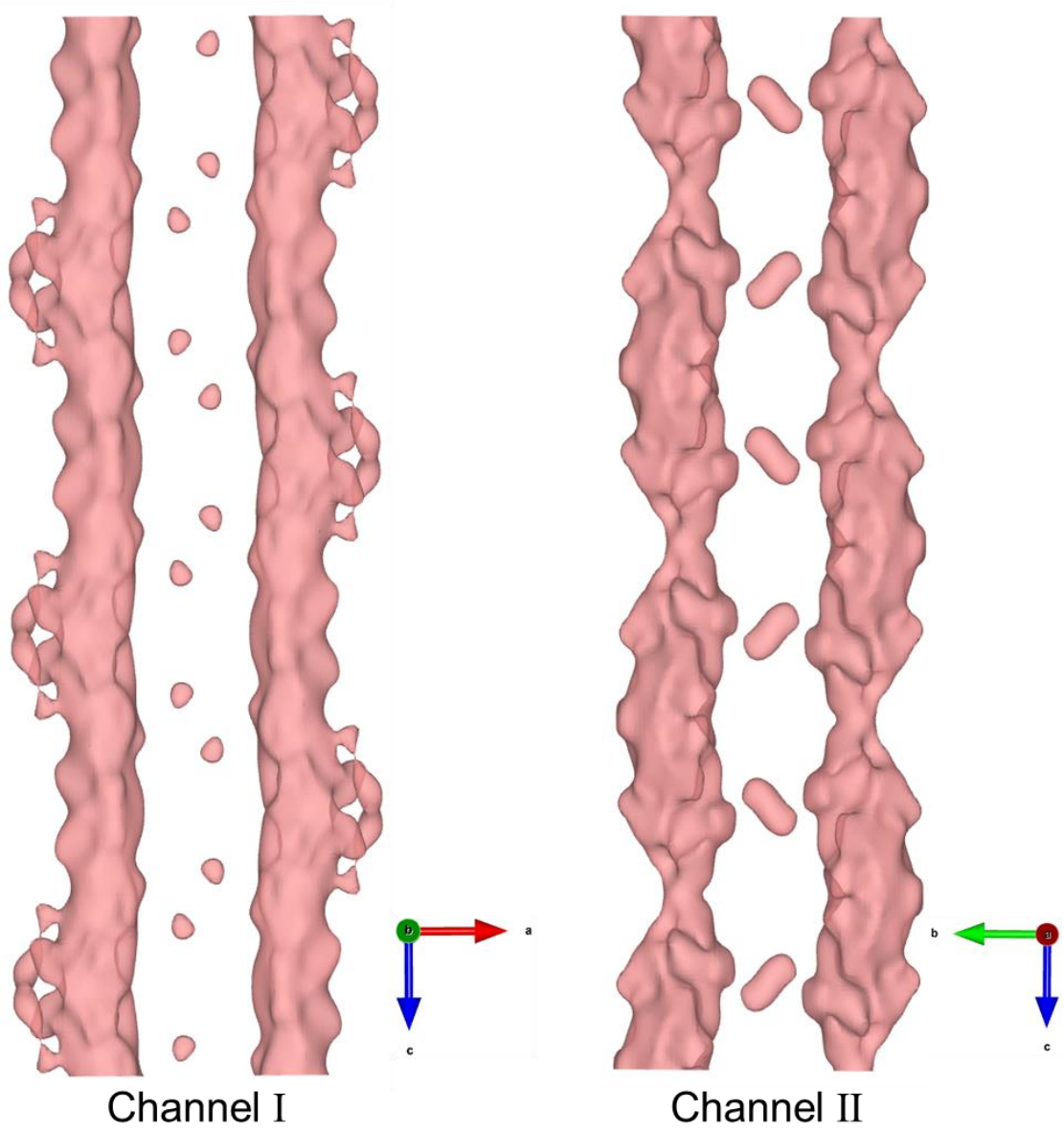

Figure S35. Color-coded 3D electron-density profile of NHA in COF-300-ip channel I (left) in *b*-axis and channel II (right) in *a*-axis. Red isosurface level represents electron density of 0.400 eÅ^3.

Table S9. Crystallography data and structure determination for NHA@COF-300-ip

Compound	NHA@COF-300-ip
Cell formula	$C_{41}H_{28}N_4 \cdot 1.3C_6H_{14}O$
Formula weight	712.89
Crystal system	Orthorhombic
Space group	$I2_12_12_1(24)$
a (Å)	24.428(12)
b (Å)	20.952(10)
c (Å)	8.282(3)
α (º)	90
β (º)	90
γ (º)	90
V (Å^3)	4239(3)
Z	4
F(000)	1517.0
Crystal density (g/cm^3)	1.117
Absorption coefficient (mm^{-1})	0.067
Crystal size (μm)	60 x 20 x 10
Temperature (K)	100
Wavelength (Å)	0.7107
2θ range for data collection	3.334/42.474
Index ranges	-24≤h≤24/-21≤k≤21/-7≤l≤7
Total/Unique data	7698/2207
R_{int} (%)	11.09
Observed data [I＞2σ(I)]	1059
R_1[I＞2σ(I)][a]	0.1278
wR_2 (all data)[b]	0.3079
S[c]	1.071
Completeness (%)	93.4
Largest diff. peak/hole (e/Å^3)	0.26/-0.28
CCDC number	2385502

[a] $R_1 = \Sigma||F_o| - |F_c||/\Sigma|F_o|$; [b] $wR_2 = [\Sigma w(F_o^2 - F_c^2)^2/\Sigma w(F_o^2)^2]^{1/2}$; [c] $S = [\Sigma w(F_o^2 - F_c^2)^2/(N_{ref} - N_{par})]^{1/2}$.

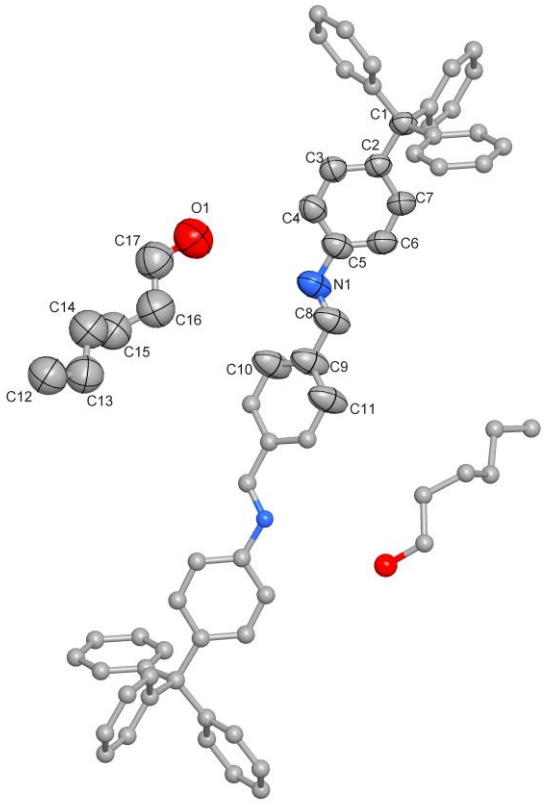

Figure S36. Thermal ellipsoid plot of the asymmetry unit for the single-crystal structure of NHA@COF-300-op (Framework with 50% probability, NHA with 20% probability; C, grey; N, blue; O, red). Hydrogen atoms were omitted for clarity; symmetry-related atoms were not labelled and represented as spheres.

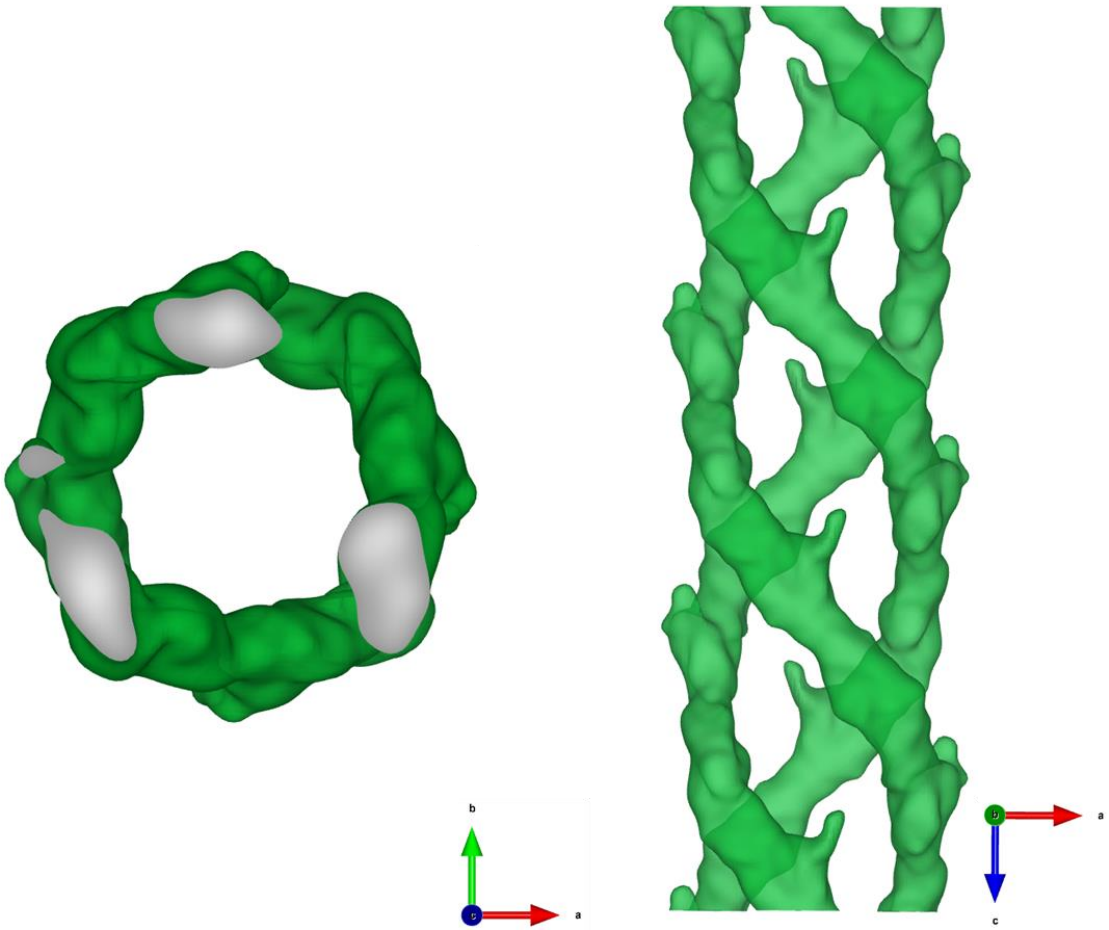

Figure S37. Color-coded 3D electron-density profile of NHA in COF-300-op *c*-axis (left) and *b*-axis (right). Green isosurface level represents electron density of 0.480 eÅ^3.

Table S10. Crystallography data and structure determination for NHA@COF-300-op

Compound	NHA@COF-300-op
Cell formula	$C_{41}H_{28}N_4 \cdot 2C_6H_{14}O$
Formula weight	840.85
Crystal system	Tetragonal
Space group	$I4_1/a$ (88)
a (Å)	25.5985(9)
b (Å)	25.5985(9)
c (Å)	7.7440(4)
α (º)	90
β (º)	90
γ (º)	90
V (Å^3)	5074.5(4)
Z	4
F(000)	1736.0
Crystal density (g/cm^3)	1.101
Absorption coefficient (mm^{-1})	0.069
Crystal size (μm)	60 x 20 x 10
Temperature (K)	100
Wavelength (Å)	0.7107
2θ range for data collection	4.5/50.036
Index ranges	-27≤h≤28/-30≤k≤30/-9≤l≤9
Total/Unique data	17107/2176
R_{int} (%)	4.35
Observed data [I＞2σ(I)]	1641
R_1[I＞2σ(I)][a]	0.1078
wR_2 (all data)[b]	0.2646
S[c]	0.988
Completeness (%)	97.2
Largest diff. peak/hole (e/Å^3)	0.25/-0.23
CCDC number	2385504

[a] $R_1 = \Sigma||F_o| - |F_c||/\Sigma|F_o|$; [b] $wR_2 = [\Sigma w(F_o^2 - F_c^2)^2/\Sigma w(F_o^2)^2]^{1/2}$; [c] $S = [\Sigma w(F_o^2 - F_c^2)^2/(N_{ref} - N_{par})]^{1/2}$.

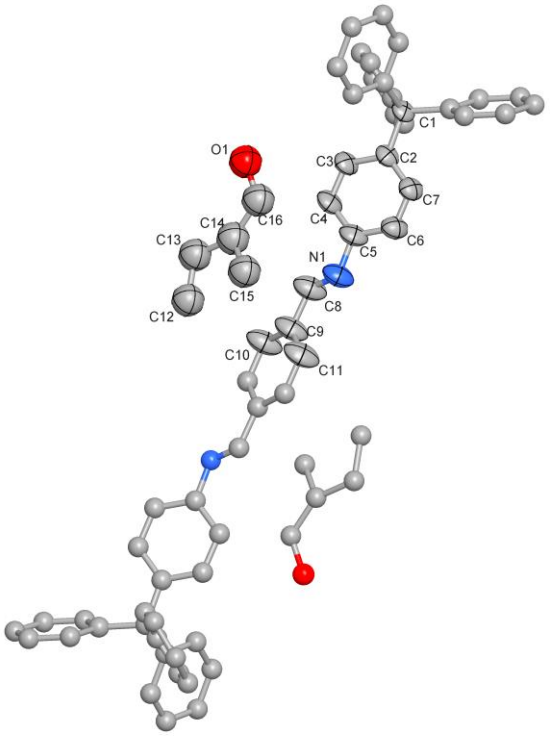

Figure S38. Thermal ellipsoid plot of the asymmetry unit for the single-crystal structure of MB@COF-300-op (Framework with 50% probability, MB with 20% probability; C, grey; N, blue; O, red). Hydrogen atoms were omitted for clarity; symmetry-related atoms were not labelled and represented as spheres.

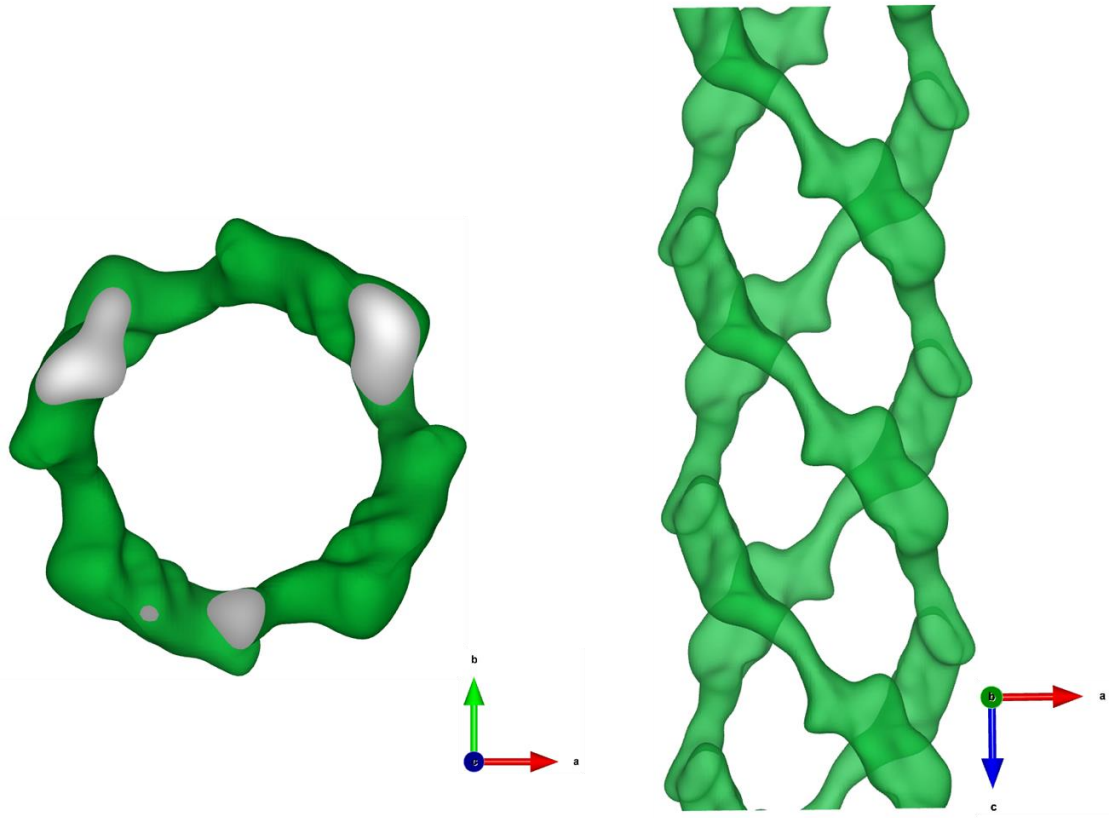

Figure S39. Color-coded 3D electron-density profile of MB in COF-300-op *c*-axis (left) and *b*-axis (right). Green isosurface level represents electron density of 0.262 eÅ^3.

Table S11. Crystallography data and structure determination for MB@COF-300-op

Compound	MB@COF-300-op
Cell formula	$C_{41}H_{28}N_4 \cdot C_5H_{12}O$
Formula weight	664.82
Crystal system	Tetragonal
Space group	$I4_1/a$ (88)
a (Å)	26.7065(11)
b (Å)	26.7065(11)
c (Å)	7.4562(4)
α (º)	90
β (º)	90
γ (º)	90
V (Å^3)	5318.0(5)
Z	4
F(000)	1408.0
Crystal density (g/cm^3)	0.830
Absorption coefficient (mm^{-1})	0.050
Crystal size (μm)	60 x 20 x 10
Temperature (K)	100
Wavelength (Å)	0.7107
2θ range for data collection	5.672/47.636
Index ranges	-28≤h≤30/-30≤k≤30/-8≤l≤8
Total/Unique data	18385/1963
R_{int} (%)	3.36
Observed data [I＞2σ(I)]	1654
R_1[I＞2σ(I)][a]	0.1003
wR_2 (all data)[b]	0.2614
S[c]	1.064
Completeness (%)	96.0
Largest diff. peak/hole (e/Å^3)	0.43/-0.24
CCDC number	2385505

[a] $R_1 = \Sigma||F_o| - |F_c||/\Sigma|F_o|$; [b] $wR_2 = [\Sigma w(F_o^2 - F_c^2)^2/\Sigma w(F_o^2)^2]^{1/2}$; [c] $S = [\Sigma w(F_o^2 - F_c^2)^2/(N_{ref} - N_{par})]^{1/2}$.

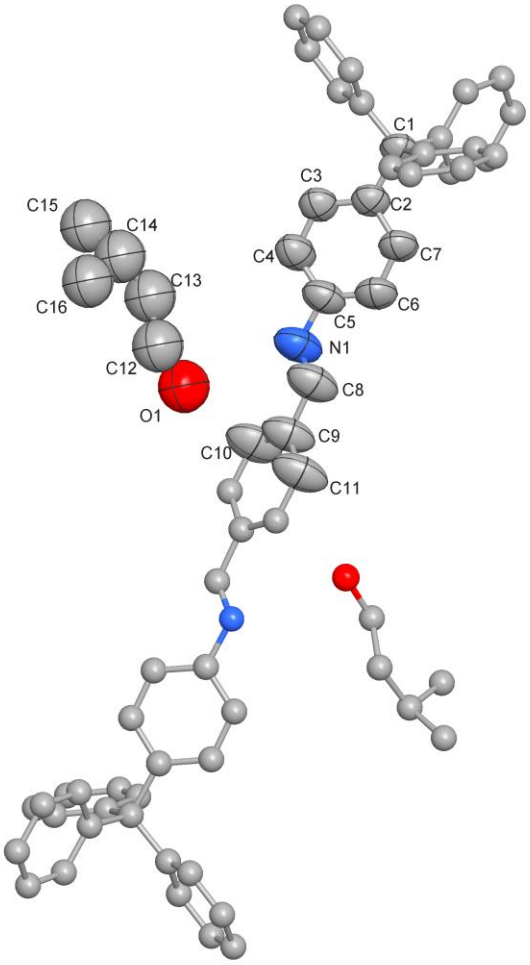

Figure S40. Thermal ellipsoid plot of the asymmetry unit for the single-crystal structure of IAA@COF-300-op (Framework with 50% probability, IAA with 25% probability; C, grey; N, blue; O, red). Hydrogen atoms were omitted for clarity; symmetry-related atoms were not labelled and represented as spheres.

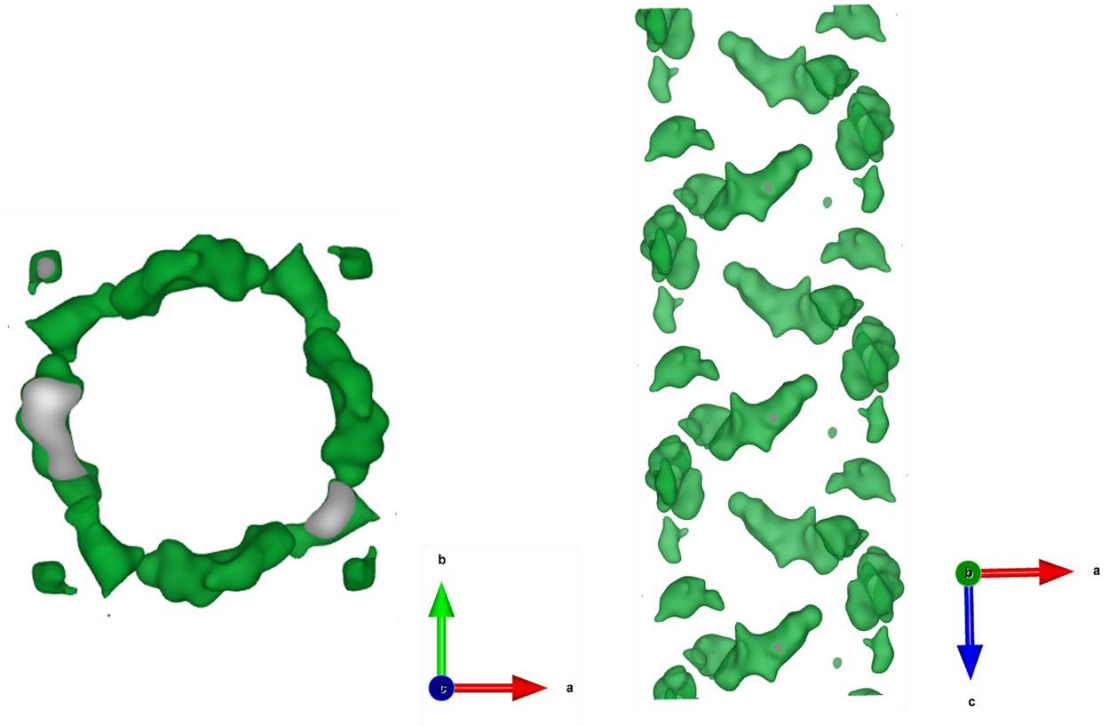

Figure S41. Color-coded 3D electron-density profile of IAA in COF-300-op *c*-axis (left) and *b*-axis (right). Green isosurface level represents electron density of 0.170 eÅ^3.

Table S12. Crystallography data and structure determination for IAA@COF-300-op

Compound	IAA@COF-300-op
Cell formula	$C_{41}H_{28}N_4 \cdot 1.33C_5H_{12}O$
Formula weight	694.20
Crystal system	Tetragonal
Space group	$I4_1/a$ (88)
a (Å)	26.0896(16)
b (Å)	26.0896(16)
c (Å)	7.6020(6)
α (º)	90
β (º)	90
γ (º)	90
V (Å^3)	5174.4(8)
Z	4
F(000)	1475.0
Crystal density (g/cm^3)	0.891
Absorption coefficient (mm^{-1})	0.054
Crystal size (μm)	60 x 20 x 10
Temperature (K)	100
Wavelength (Å)	0.7107
2θ range for data collection	5.672/47.636
Index ranges	-32≤h≤33/-29≤k≤33/-8≤l≤9
Total/Unique data	16426/2745
R_{int} (%)	3.28
Observed data [I＞2σ(I)]	1566
R_1[I＞2σ(I)][a]	0.1039
wR_2 (all data)[b]	0.2580
S[c]	0.944
Completeness (%)	96.4
Largest diff. peak/hole (e/Å^3)	0.21/-0.14
CCDC number	2385506

[a] $R_1 = \Sigma||F_o| - |F_c||/\Sigma|F_o|$; [b] $wR_2 = [\Sigma w(F_o^2 - F_c^2)^2/\Sigma w(F_o^2)^2]^{1/2}$; [c] $S = [\Sigma w(F_o^2 - F_c^2)^2/(N_{ref} - N_{par})]^{1/2}$.

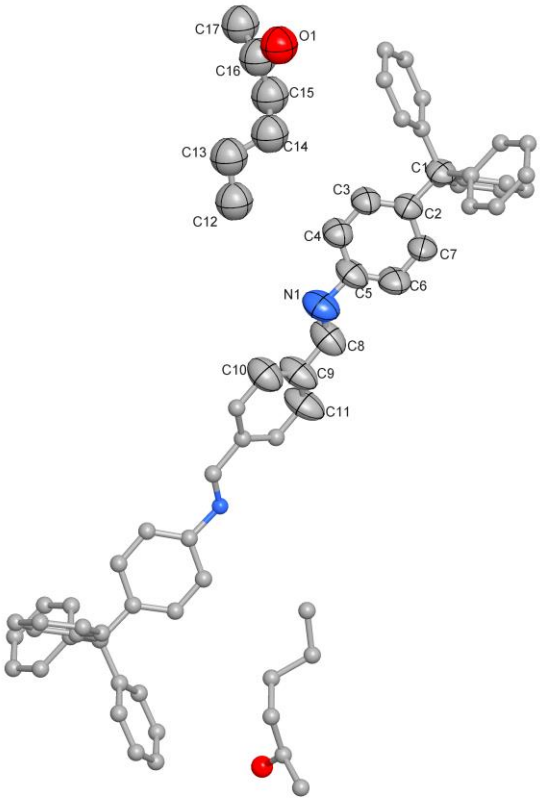

Figure S42. Thermal ellipsoid plot of the asymmetry unit for the single-crystal structure of SPA@COF-300-op (Framework with 50% probability, SPA with 20% probability; C, grey; N, blue; O, red). Hydrogen atoms were omitted for clarity; symmetry-related atoms were not labelled and represented as spheres.

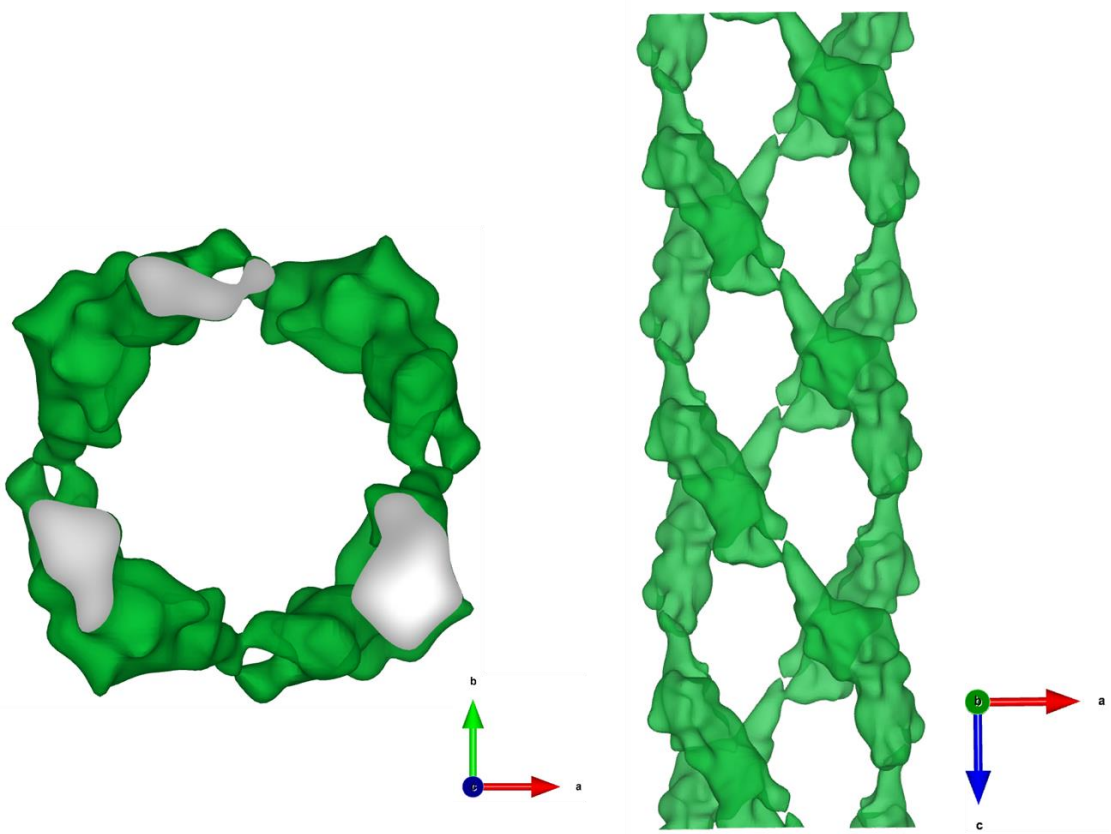

Figure S43. Color-coded 3D electron-density profile of SPA in COF-300-op *c*-axis (left) and *b*-axis (right). Green isosurface level represents electron density of 0.293 eÅ^3.

Table S13. Crystallography data and structure determination for SPA@COF-300-op

Compound	SPA@COF-300-op
Cell formula	$C_{41}H_{28}N_4 \cdot 1.3C_5H_{12}O$
Formula weight	712.89
Crystal system	Tetragonal
Space group	$I4_1/a$ (88)
a (Å)	26.355(5)
b (Å)	26.355(5)
c (Å)	7.709(2)
α (º)	90
β (º)	90
γ (º)	90
V (Å^3)	5355(2)
Z	4
F(000)	1517.0
Crystal density (g/cm^3)	0.884
Absorption coefficient (mm^{-1})	0.053
Crystal size (μm)	60 x 20 x 10
Temperature (K)	100
Wavelength (Å)	0.7107
2θ range for data collection	6.184/45.426
Index ranges	-27≤h≤28/-27≤k≤28/-7≤l≤8
Total/Unique data	7615/1679
R_{int} (%)	5.71
Observed data [I＞2σ(I)]	1106
R_1[I＞2σ(I)][a]	0.1470
wR_2 (all data)[b]	0.3752
S[c]	1.060
Completeness (%)	93.3
Largest diff. peak/hole (e/Å^3)	0.29/-0.18
CCDC number	2385507

[a] $R_1 = \Sigma||F_o| - |F_c||/\Sigma|F_o|$; [b] $wR_2 = [\Sigma w(F_o^2 - F_c^2)^2/\Sigma w(F_o^2)^2]^{1/2}$; [c] $S = [\Sigma w(F_o^2 - F_c^2)^2/(N_{ref} - N_{par})]^{1/2}$.

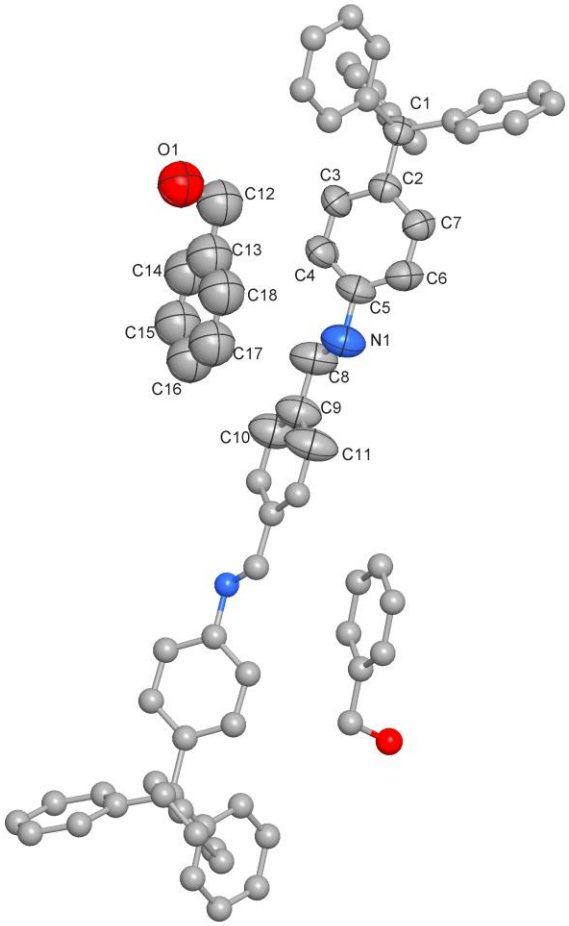

Figure S44. Thermal ellipsoid plot of the asymmetry unit for the single-crystal structure of BA@COF-300-op (Framework with 50% probability, BA with 20% probability; C, grey; N, blue; O, red). Hydrogen atoms were omitted for clarity; symmetry-related atoms were not labelled and represented as spheres.

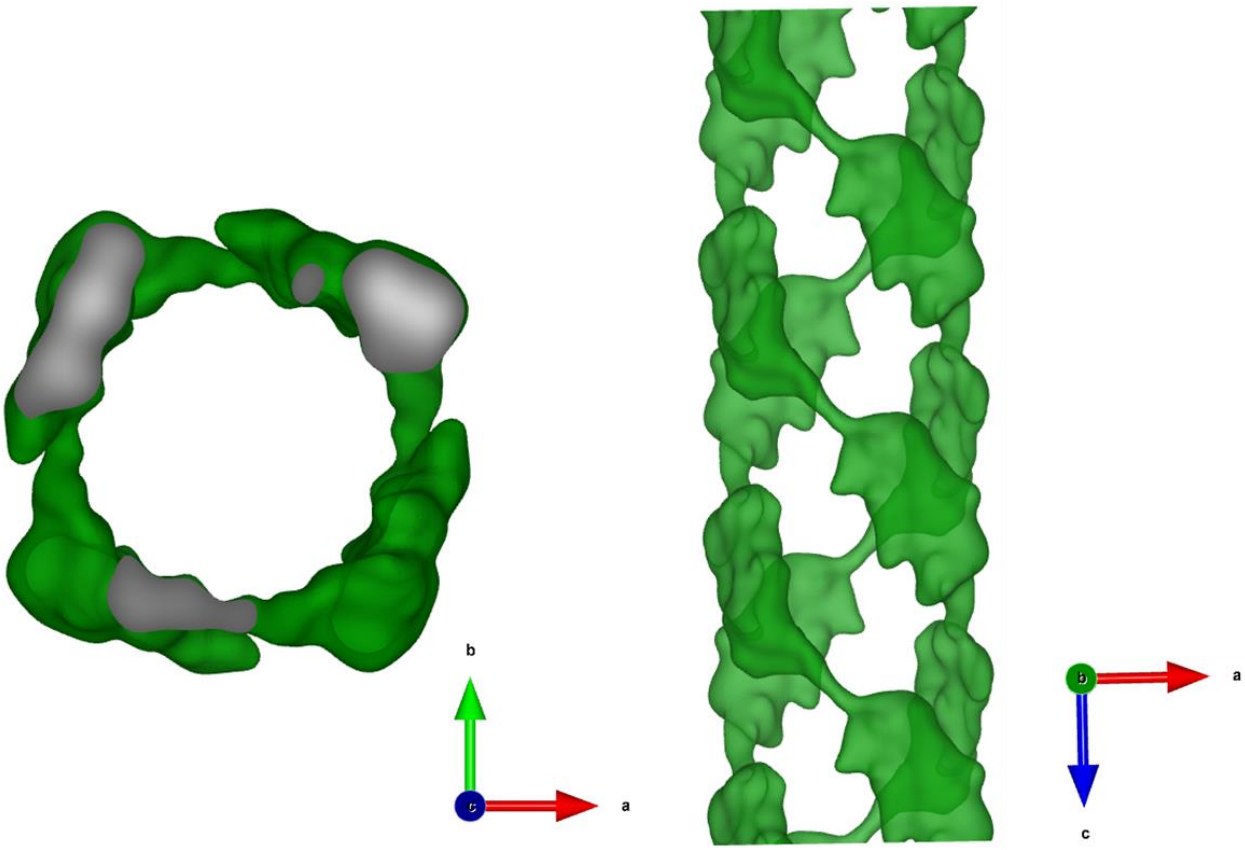

Figure S45. Color-coded 3D electron-density profile of BA in COF-300-op *c*-axis (left) and *b*-axis (right). Green isosurface level represents electron density of 0.364 eÅ^3.

Table S14. Crystallography data and structure determination for BA@COF-300-op

Compound	BA@COF-300-op
Cell formula	$C_{41}H_{28}N_4 \cdot 1.3C_7H_8O$
Formula weight	720.83
Crystal system	Tetragonal
Space group	$I4_1/a$ (88)
a (Å)	26.213(4)
b (Å)	26.213(4)
c (Å)	7.5202(16)
α (º)	90
β (º)	90
γ (º)	90
V (Å^3)	5167.3(18)
Z	4
F(000)	1517.0
Crystal density (g/cm^3)	0.927
Absorption coefficient (mm^{-1})	0.056
Crystal size (μm)	60 x 20 x 10
Temperature (K)	100
Wavelength (Å)	0.7107
2θ range for data collection	5.636/43.44
Index ranges	-26≤h≤27/-25≤k≤27/-7≤l≤7
Total/Unique data	7025/1459
R_{int} (%)	5.54
Observed data [I＞2σ(I)]	1177
R_1[I＞2σ(I)][a]	0.1482
wR_2 (all data)[b]	0.3569
S[c]	1.070
Completeness (%)	95.0
Largest diff. peak/hole (e/Å^3)	0.45/-0.27
CCDC number	2385508

[a] $R_1 = \Sigma||F_o| - |F_c||/\Sigma|F_o|$; [b] $wR_2 = [\Sigma w(F_o^2 - F_c^2)^2/\Sigma w(F_o^2)^2]^{1/2}$; [c] $S = [\Sigma w(F_o^2 - F_c^2)^2/(N_{ref} - N_{par})]^{1/2}$.

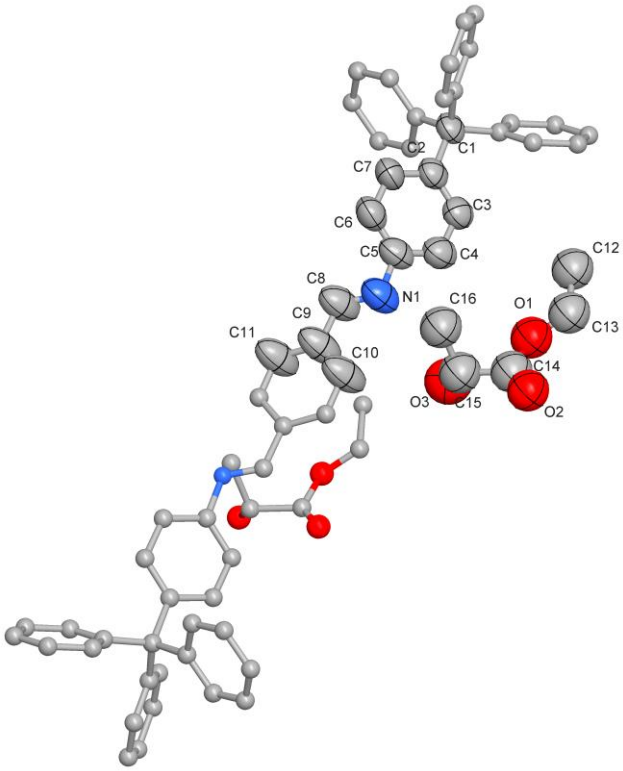

Figure S46. Thermal ellipsoid plot of the asymmetry unit for the single-crystal structure of EL@COF-300-op (Framework with 50% probability, ethyl propionate with 20% probability; C, grey; N, blue; O, red). Hydrogen atoms were omitted for clarity; symmetry-related atoms were not labelled and represented as spheres.

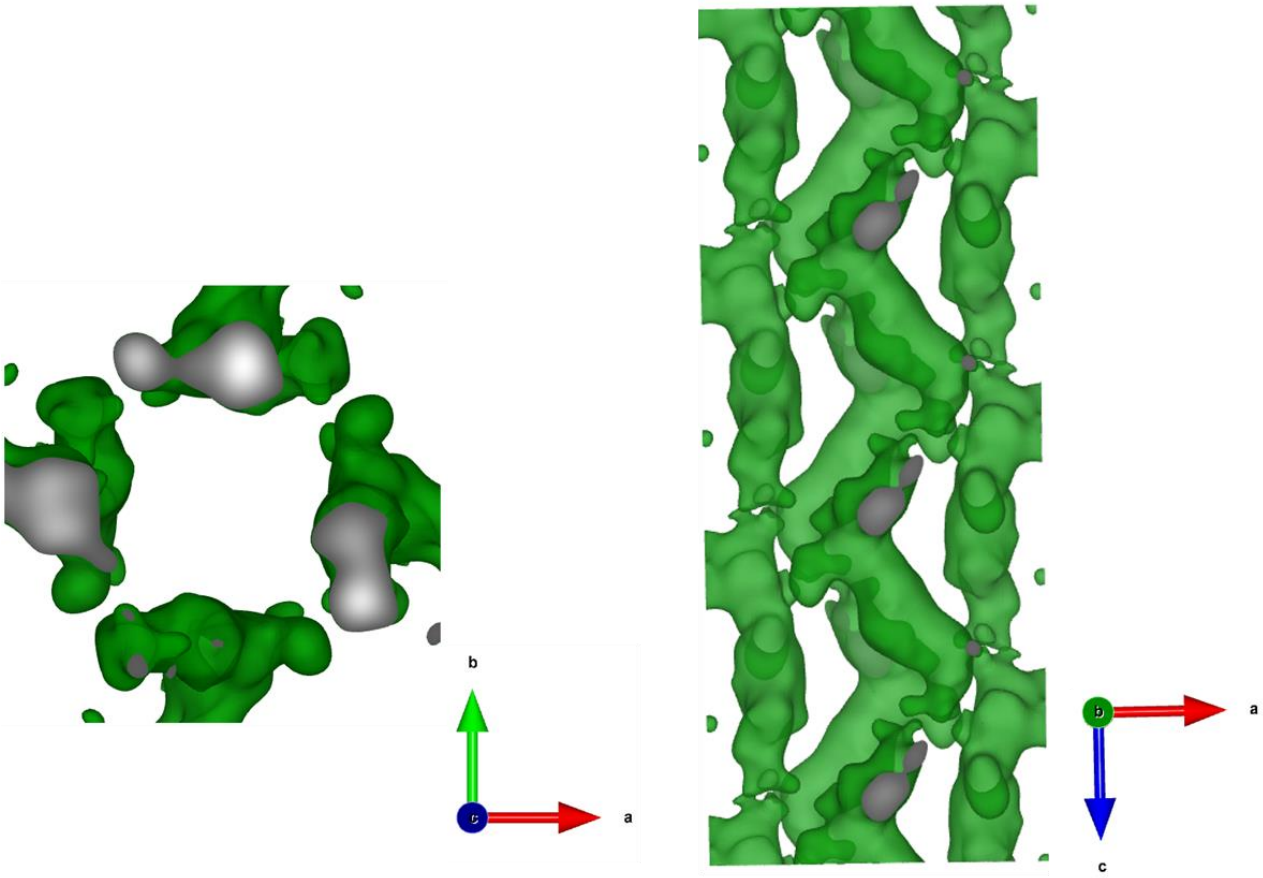

Figure S47. Color-coded 3D electron-density profile of EL in COF-300-op *c*-axis (left) and *b*-axis (right). Green isosurface level represents electron density of 0.205 eÅ^3.

Table S15. Crystallography data and structure determination for EL@COF-300-op

Compound	EL@COF-300-op
Cell formula	$C_{41}H_{28}N_4 \cdot 2C_5H_{10}O$
Formula weight	795.92
Crystal system	Tetragonal
Space group	$I4_1/a$ (88)
a (Å)	25.5006(9)
b (Å)	25.5006(9)
c (Å)	7.7420(4)
α (º)	90
β (º)	90
γ (º)	90
V (Å^3)	5034.5(4)
Z	4
F(000)	1684.0
Crystal density (g/cm^3)	1.050
Absorption coefficient (mm^{-1})	0.068
Crystal size (μm)	60 x 20 x 10
Temperature (K)	100
Wavelength (Å)	0.7107
2θ range for data collection	7.146/49.426
Index ranges	-30≤h≤29/-29≤k≤29/-9≤l≤9
Total/Unique data	18795/2082
R_{int} (%)	4.03
Observed data [I＞2σ(I)]	1556
R_1[I＞2σ(I)][a]	0.1139
wR_2 (all data)[b]	0.2887
S[c]	0.922
Completeness (%)	97.0
Largest diff. peak/hole (e/Å^3)	0.16/-0.15
CCDC number	2385509

[a] $R_1 = \Sigma||F_o| - |F_c||/\Sigma|F_o|$; [b] $wR_2 = [\Sigma w(F_o^2 - F_c^2)^2/\Sigma w(F_o^2)^2]^{1/2}$; [c] $S = [\Sigma w(F_o^2 - F_c^2)^2/(N_{ref} - N_{par})]^{1/2}$.

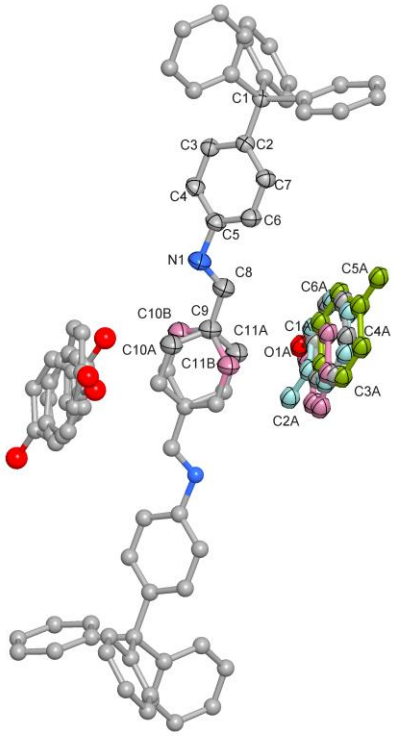

Figure S48. Thermal ellipsoid plot of the asymmetry unit for the single-crystal structure of PO@COF-300-op (Framework with 50% probability, phenol with 30% probability; C, grey; N, blue; O, red). Hydrogen atoms were omitted for clarity; symmetry-related atoms were not labelled and represented as spheres. The PO molecules are disordered, and four phenol molecules were resolved. The first phenol has an occupancy of 40%. The second PO was marked in pink, with an occupancy of 20%. The third PO was marked in blue, with an occupancy of 20%. The fourth PO was marked in green, with an occupancy of 20%. The disorder in the framework was marked in pink, with an occupancy of 0.06%.

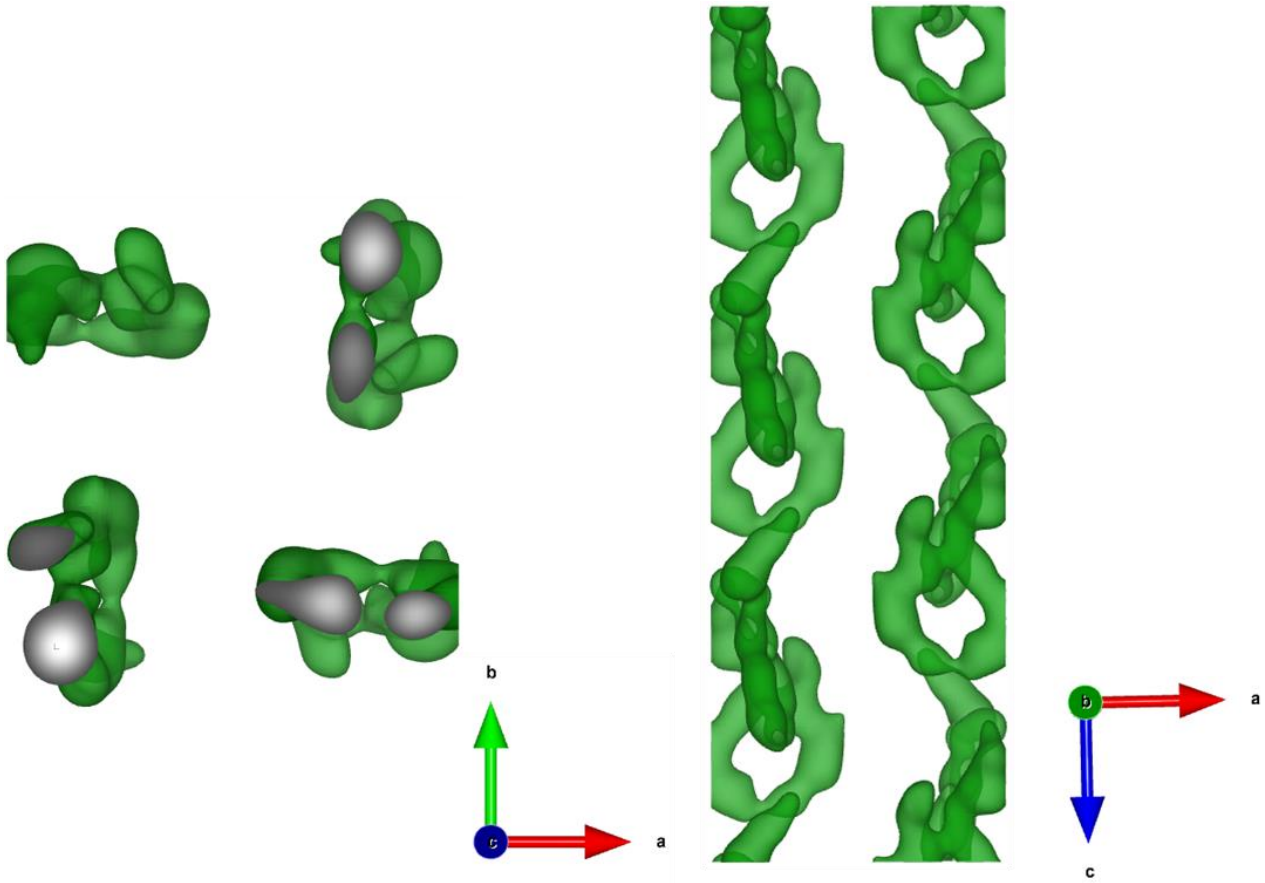

Figure S49. Color-coded 3D electron-density profile of PO in COF-300-op *c*-axis (left) and *b*-axis (right). Green isosurface level represents electron density of 0.658 eÅ^3.

Table S16. Crystallography data and structure determination for PO@COF-300-op

Compound	PO@COF-300-op
Cell formula	$C_{41}H_{28}N_4 \cdot 4C_6H_6O$
Formula weight	953.10
Crystal system	Tetragonal
Space group	$I4_1/a$ (88)
a (Å)	27.1795(13)
b (Å)	27.1795(13)
c (Å)	7.2985(4)
α (º)	90
β (º)	90
γ (º)	90
V (Å^3)	5391.6(6)
Z	4
F(000)	2008.0
Crystal density (g/cm^3)	1.174
Absorption coefficient (mm^{-1})	0.073
Crystal size (μm)	60 x 20 x 10
Temperature (K)	100
Wavelength (Å)	0.7107
2θ range for data collection	4.238/46.506
Index ranges	-28≤h≤30/-30≤k≤30/-7≤l≤7
Total/Unique data	12930/1883
R_{int} (%)	8.28
Observed data [I＞2σ(I)]	1502
R_1[I＞2σ(I)][a]	0.0951
wR_2 (all data)[b]	0.2683
S[c]	1.073
Completeness (%)	97.2
Largest diff. peak/hole (e/Å^3)	0.37/-0.27
CCDC number	2385510

[a] $R_1 = \Sigma||F_o| - |F_c||/\Sigma|F_o|$; [b] $wR_2 = [\Sigma w(F_o^2 - F_c^2)^2/\Sigma w(F_o^2)^2]^{1/2}$; [c] $S = [\Sigma w(F_o^2 - F_c^2)^2/(N_{ref} - N_{par})]^{1/2}$.

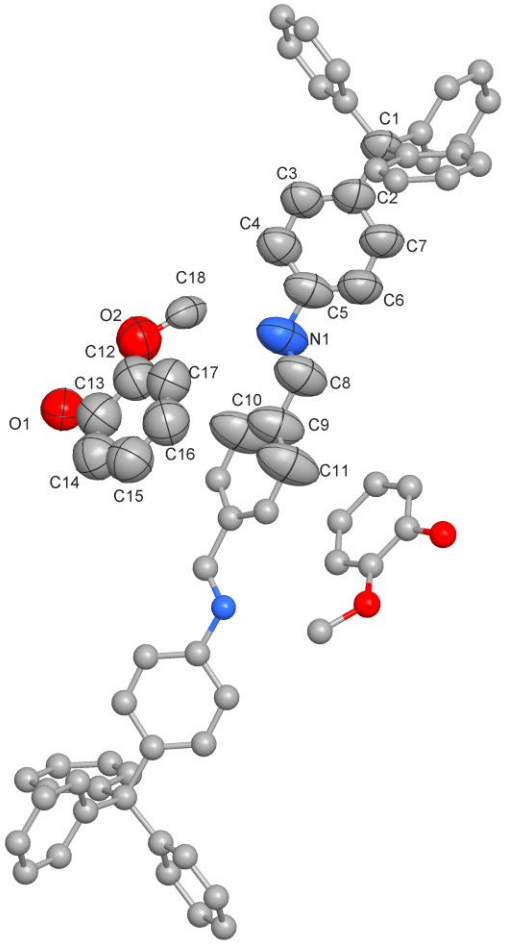

Figure S50. Thermal ellipsoid plot of the asymmetry unit for the single-crystal structure of GA@COF-300-op (Framework with 50% probability, GA with 20% probability; C, grey; N, blue; O, red). Hydrogen atoms were omitted for clarity; symmetry-related atoms were not labelled and represented as spheres.

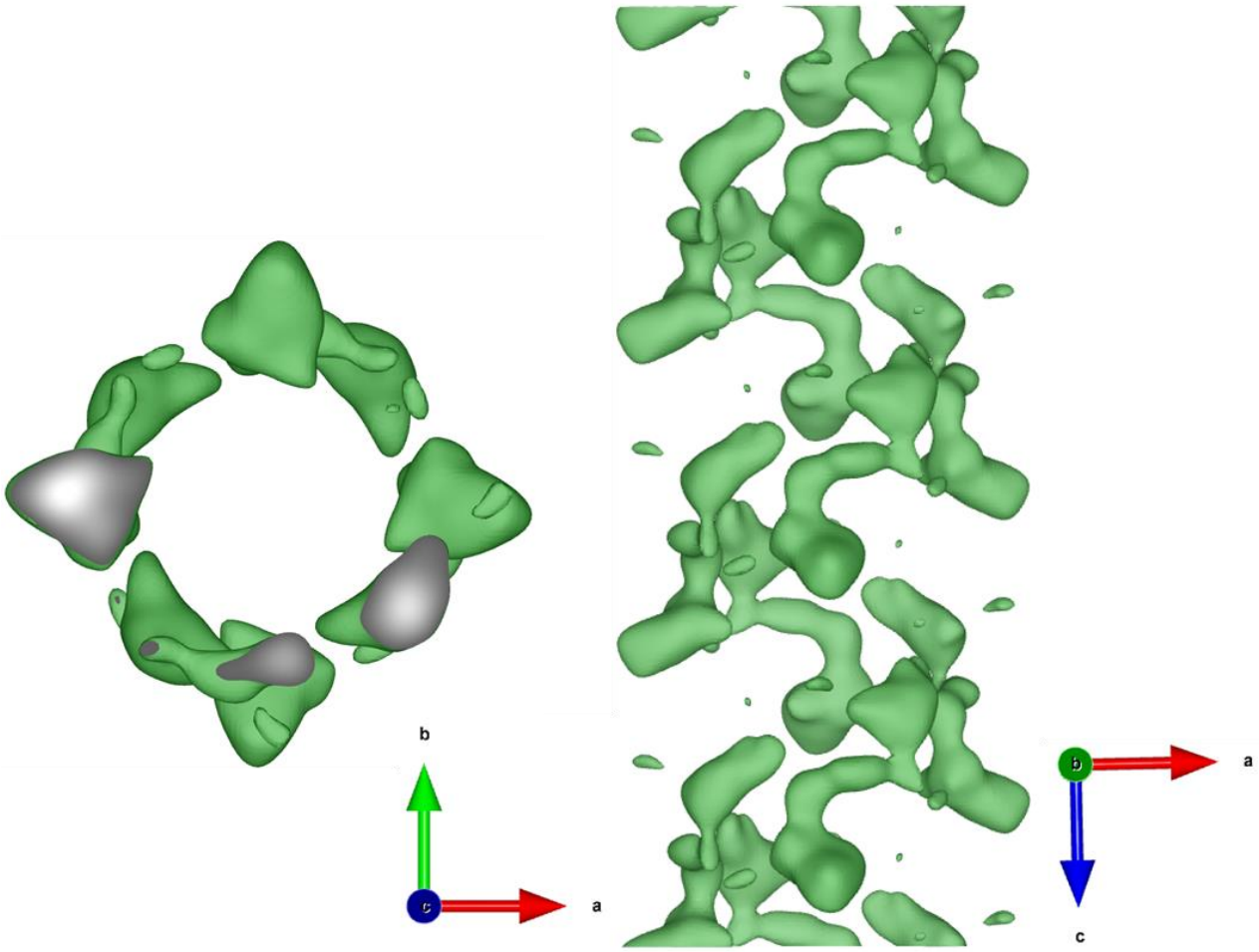

Figure S51. Color-coded 3D electron-density profile of GA in COF-300-op *c*-axis (left) and *b*-axis (right). Green isosurface level represents electron density of 0.305 eÅ^3.

Table S17. Crystallography data and structure determination for GA@COF-300-op

Compound	GA@COF-300-op
Cell formula	$C_{41}H_{28}N_4{\cdot}2C_7O_2$
Formula weight	808.81
Crystal system	Tetragonal
Space group	$I4_1/a$ (88)
a (Å)	25.5960(11)
b (Å)	25.5960(11)
c (Å)	7.7013(5)
α (º)	90
β (º)	90
γ (º)	90
V (Å^3)	5045.5(5)
Z	4
F(000)	1672.0
Crystal density (g/cm^3)	1.065
Absorption coefficient (mm^{-1})	0.068
Crystal size (μm)	60 x 20 x 10
Temperature (K)	100
Wavelength (Å)	0.7107
2θ range for data collection	7.120/49.432
Index ranges	-29≤h≤29/-30≤k≤28/-9≤l≤9
Total/Unique data	18853/2089
R_{int} (%)	3.10
Observed data [I＞2σ(I)]	1349
R_1[I＞2σ(I)][a]	0.1482
wR_2 (all data)[b]	0.3512
S[c]	0.975
Completeness (%)	97.2
Largest diff. peak/hole (e/Å^3)	0.22/-0.20
CCDC number	2385511

[a] $R_1 = \Sigma||F_o| - |F_c||/\Sigma|F_o|$; [b] $wR_2 = [\Sigma w(F_o^2 - F_c^2)^2/\Sigma w(F_o^2)^2]^{1/2}$; [c] $S = [\Sigma w(F_o^2 - F_c^2)^2/(N_{ref} - N_{par})]^{1/2}$.

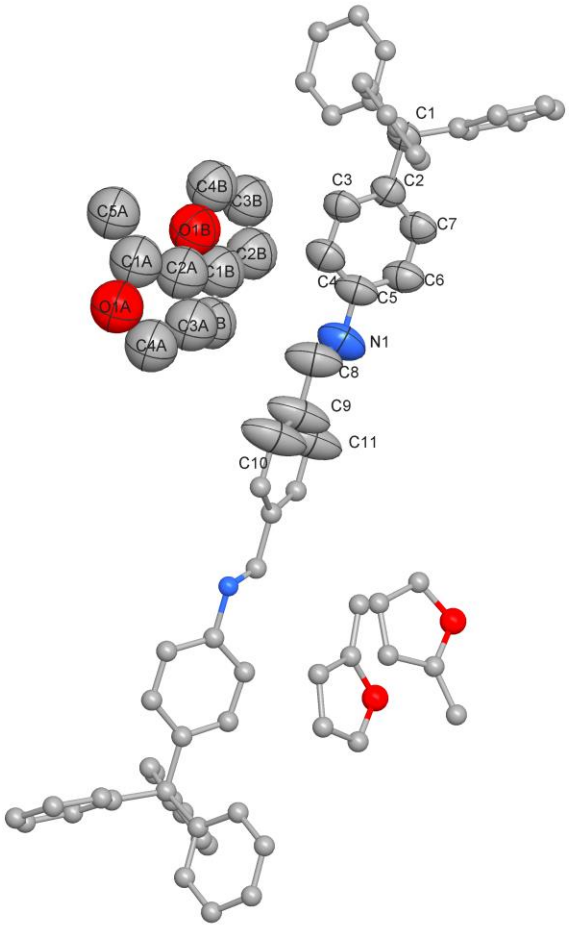

Figure S52. Thermal ellipsoid plot of the asymmetry unit for the single-crystal structure of MF@COF-300-op (Framework with 50% probability, MF with 10% probability; C, grey; N, blue; O, red). Hydrogen atoms were omitted for clarity; symmetry-related atoms were not labelled and represented as spheres.

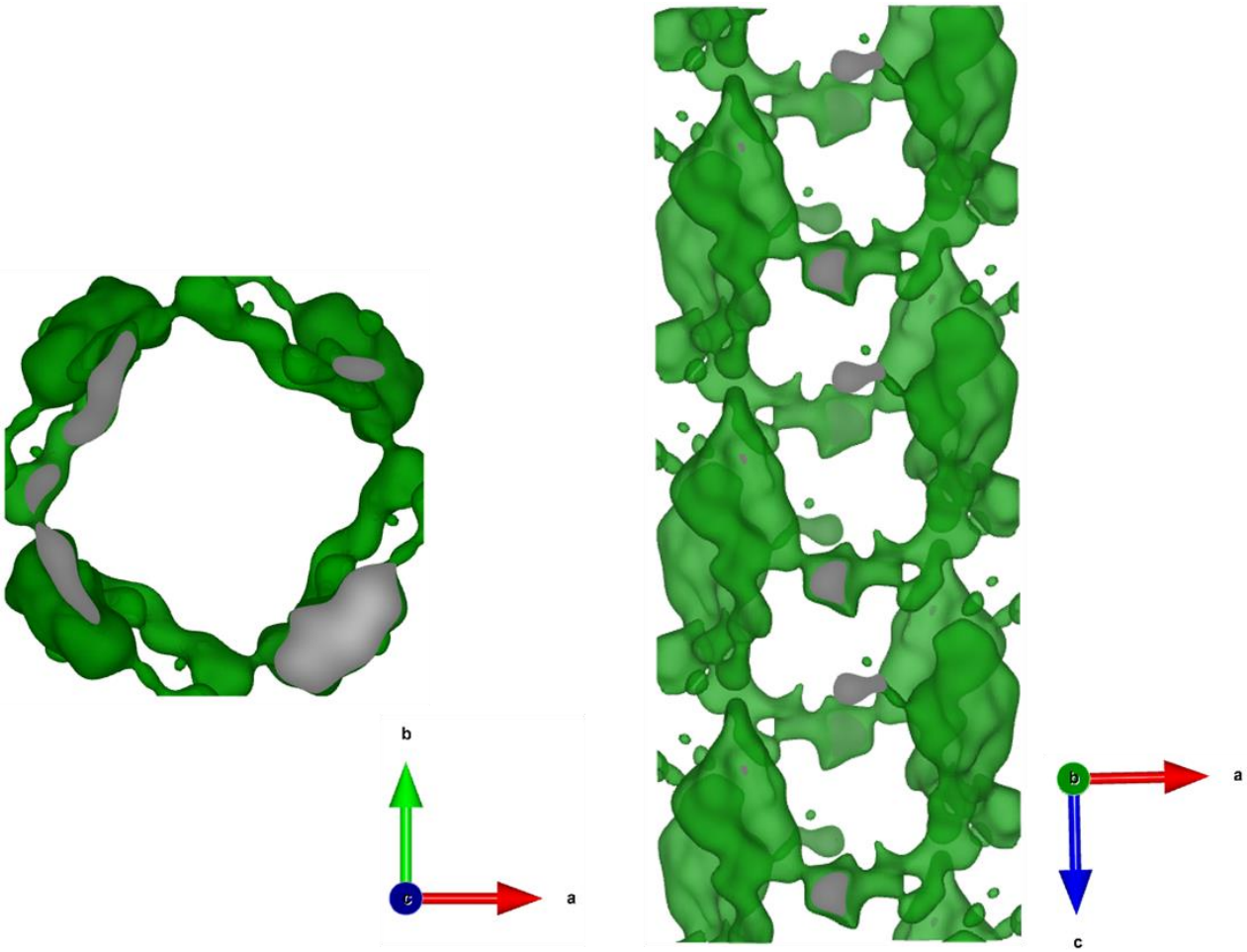

Figure S53. Color-coded 3D electron-density profile of MF in COF-300-op *c*-axis (left) and *b*-axis (right). Green isosurface level represents electron density of 0.263 eÅ^3.

Table S18. Crystallography data and structure determination for MF@COF-300-op

Compound	MF@COF-300-op
Cell formula	$C_{41}H_{28}N_4 \cdot 4C_5H_6O$
Formula weight	905.06
Crystal system	Tetragonal
Space group	$I4_1/a$ (88)
a (Å)	26.871(4)
b (Å)	26.871(4)
c (Å)	7.4031(15)
α (º)	90
β (º)	90
γ (º)	90
V (Å^3)	5345.5(19)
Z	4
F(000)	1912.0
Crystal density (g/cm^3)	1.125
Absorption coefficient (mm^{-1})	0.071
Crystal size (μm)	60 x 20 x 10
Temperature (K)	100
Wavelength (Å)	0.7107
2θ range for data collection	4.288/43.43
Index ranges	-27≤h≤27/-27≤k≤27/-7≤l≤7
Total/Unique data	16596/1562
R_{int} (%)	5.67
Observed data [I＞2σ(I)]	1101
R_1[I＞2σ(I)][a]	0.1262
wR_2 (all data)[b]	0.2695
S[c]	0.980
Completeness (%)	98.7
Largest diff. peak/hole (e/Å^3)	0.14/-0.12
CCDC number	2385512

[a] $R_1 = \Sigma||F_o| - |F_c||/\Sigma|F_o|$; [b] $wR_2 = [\Sigma w(F_o^2 - F_c^2)^2/\Sigma w(F_o^2)^2]^{1/2}$; [c] $S = [\Sigma w(F_o^2 - F_c^2)^2/(N_{ref} - N_{par})]^{1/2}$.

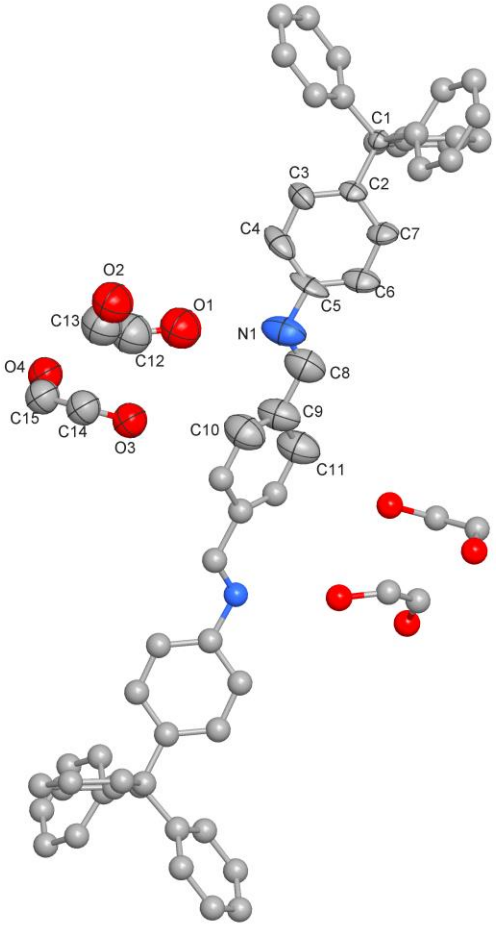

Figure S54. Thermal ellipsoid plot of the asymmetry unit for the single-crystal structure of EG@COF-300-op (Framework with 50% probability, EG with 30% probability; C, grey; N, blue; O, red). Hydrogen atoms were omitted for clarity; symmetry-related atoms were not labelled and represented as spheres.

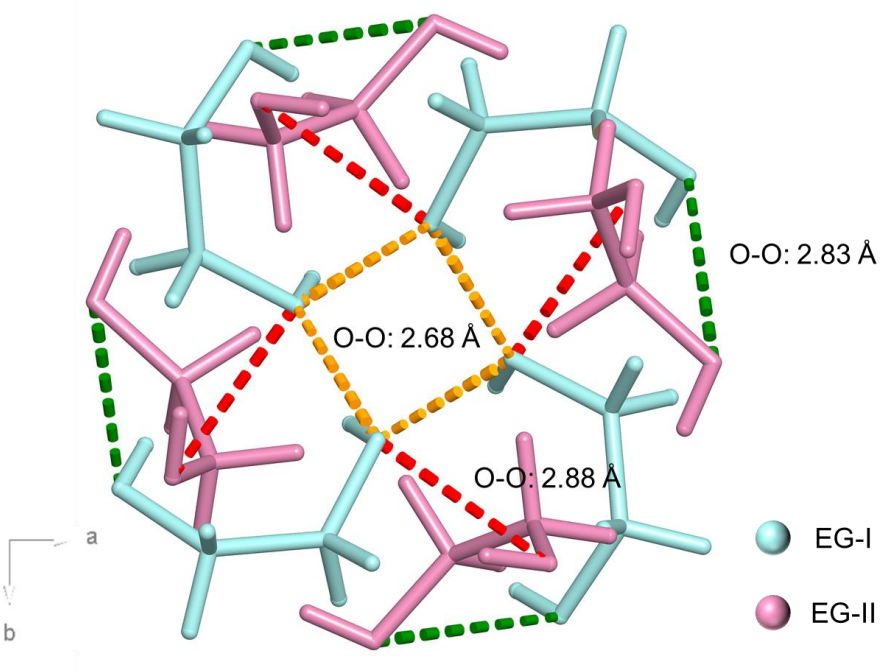

Figure S55. The interaction between EG molecules (EG-I colored with cyan, and EG-II colored with purple). EG molecules are connected by hydrogen bonds. For the EG-I molecule, the O-O distance is 2.68 Å (orange dotted line), indicates that there is a spiral hydrogen chain. EG-I and EG-II molecules form hydrogen bonds with O-O distances of 2.83 Å (green dotted line) and 2.88 Å (red dotted line), respectively.

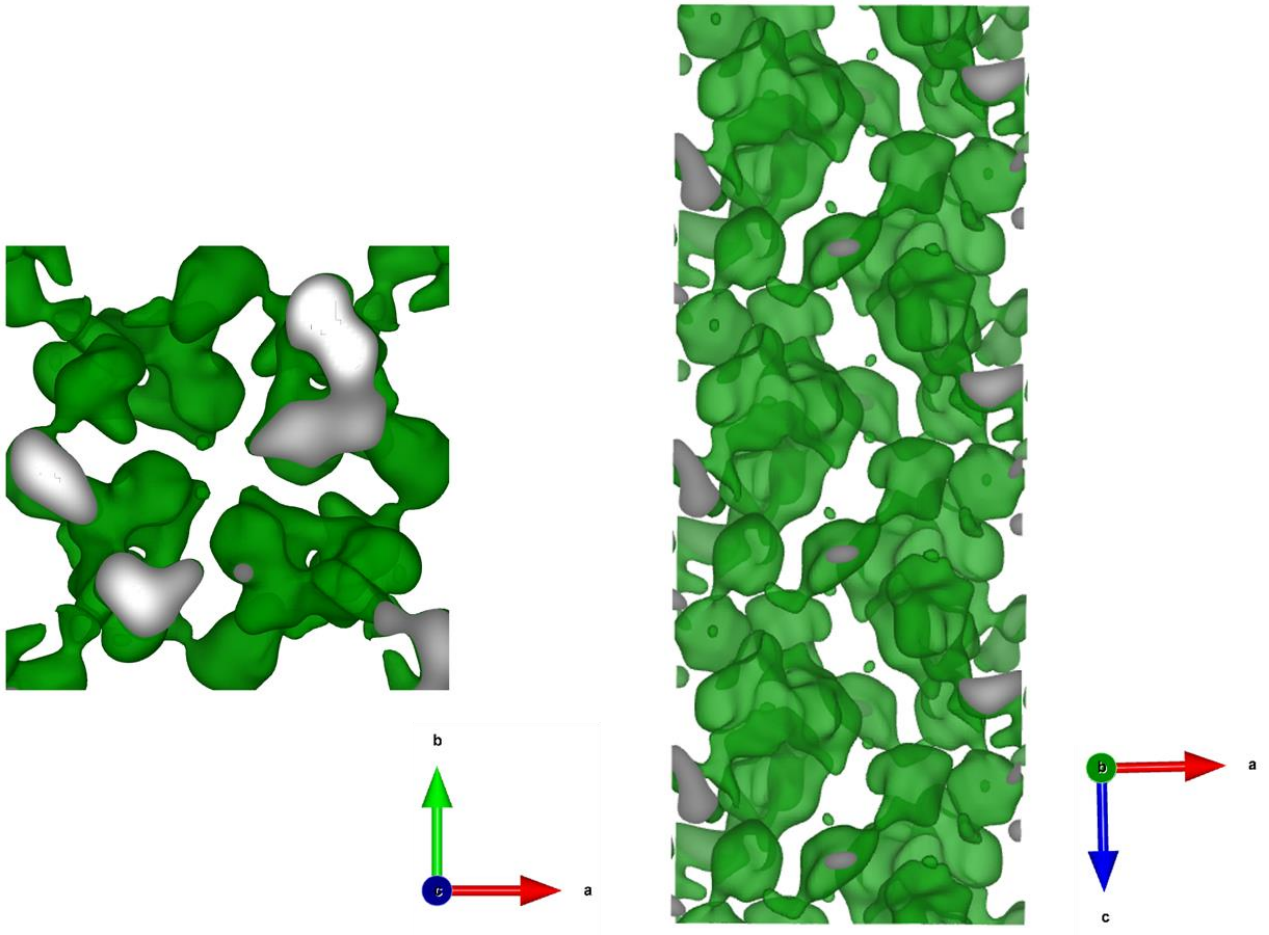

Figure S56. Color-coded 3D electron-density profile of EG in COF-300-op *c*-axis (left) and *b*-axis (right). Green isosurface level represents electron density of 0.300 eÅ^3.

Table S19. Crystallography data and structure determination for EG@COF-300-op

Compound	EG@COF-300-op
Cell formula	$C_{41}H_{28}N_4 \cdot 2.6C_2H_6O_2$
Formula weight	742.16
Crystal system	Tetragonal
Space group	$I4_1/a$ (88)
a (Å)	25.0829(13)
b (Å)	25.0829(13)
c (Å)	7.8582(6)
α (º)	90
β (º)	90
γ (º)	90
V (Å^3)	4944.0(6)
Z	4
F(000)	1571.0
Crystal density (g/cm^3)	0.997
Absorption coefficient (mm^{-1})	0.062
Crystal size (μm)	60 x 20 x 10
Temperature (K)	100
Wavelength (Å)	0.6888
2θ range for data collection	4.452/40.676
Index ranges	-25≤h≤25/-25≤k≤25/-7≤l≤7
Total/Unique data	8247/1293
R_{int} (%)	4.93
Observed data [I＞2σ(I)]	1147
R_1[I＞2σ(I)][a]	21.57
wR_2 (all data)[b]	43.83
S[c]	0.952
Completeness (%)	96.9
Largest diff. peak/hole (e/Å^3)	0.52/-0.38
CCDC number	2385513

[a] $R_1 = \Sigma||F_o| - |F_c||/\Sigma|F_o|$; [b] $wR_2 = [\Sigma w(F_o^2 - F_c^2)^2/\Sigma w(F_o^2)^2]^{1/2}$; [c] $S = [\Sigma w(F_o^2 - F_c^2)^2/(N_{ref} - N_{par})]^{1/2}$.

Table S20. Single Crystal data information for all guest@COF-300

Guest	Space group	Crystal cell	Resolution (Å)	Complete (%)
NBA	-ip, $I2_12_12_1$	a=24.301(10) b=20.762(8) c=8.172(3) V=4123.08Å^3	0.96	89.8
	-op, $I4_1/a$	a=25.4066(13) c=7.7749(6) V=5021.6Å^3	0.80	97.0
NPA	-ip, $I2_12_12_1$	a=24.177(6) b=20.366(5) c=8.3463(17) V=4109.5Å^3	0.92	94.7
	-op, $I4_1/a$	a=25.3950(11) c=7.7964(5) V=5027.9Å^3	0.85	96.5
NHA	-ip, $I2_12_12_1$	a=24.428(12) b=20.952(10) c=8.282(3) V=4239.0Å^3	0.98	93.4
	-op, $I4_1/a$	a=25.5985(9) c=7.7440(4) V=5074.5Å^3	0.84	97.2
MB	-op, $I4_1/a$	a=26.871(4) c=7.4031(15) V=5345.5Å^3	0.96	98.7
IAA	-op, $I4_1/a$	a=26.0896(16) c=7.6020(6) V=5174.4Å^3	0.78	96.4
SPA	-op, $I4_1/a$	a=26.355(5) c=7.709(2) V=5355.0Å^3	0.92	93.3
BA	-op, $I4_1/a$	a=26.213(4) c=7.5202(16) V=5167.3Å^3	0.96	95.0
EL	-op, $I4_1/a$	a=25.5006(9) c=7.7420(4) V=5034.5Å^3	0.85	97.0
PO	-op, $I4_1/a$	a=27.1795(13) c=7.2985(4) V=5391.6Å^3	0.90	97.2
GA	-op, $I4_1/a$	a=25.596(11) c=7.701(5) V=5045.5Å^3	0.85	91.5
MF	-op, $I4_1/a$	a=26.7065(11) c=7.4562(4) V=5318.0Å^3	0.95	96.6
EG	-op, $I4_1/a$	a=25.083(13) c=7.858(6) V=4944.0Å^3	0.99	96.9

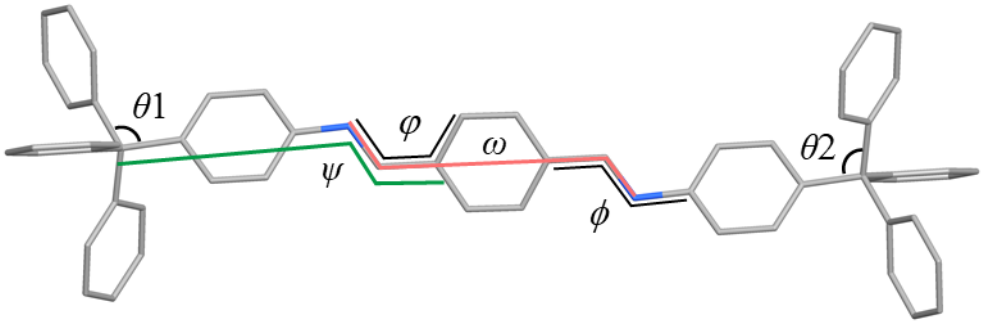

Figure S57. Definition of degree of freedom of COF-300 structure.

Table S21. Variation in conformational degree of freedom in COF-300 different phase

Guest	Guest (mol/mol)	θ1 (º)	θ2(º)	ω(º)	ψ (º)	φ (º)	ϕ (º)	Node distance (Å)
NBA	2 (-ip)	102.717/ 103.200	111.542/ 114.114	0.495/ 132.995	-163.737/ -176.616	-2.610/ -15.941	172.902/ -178.172	18.167/ 18.307
	4 (-op)	105.446	111.521	180	-178.70	9.78	179.40	18.693
NPA	1.5 (-ip)	101.851/ 103.993	113.359/ 112.316	-0.776/ -133.944	-163.071/ 176.035	3.060/ 20.018	-172.210/ -178.275	18.333/ 18.472
	3 (-op)	103.933	112.278	-180	179.446	10.606	179.435	18.638
NHA	1.3 (-ip)	101.762/ 104.000	113.136/ 112.580	4.521/ -134.416	-163.687/ 175.647	4.682/ 17.125	-172.734/ 177.812	18.397/ 18.477
	3 (-op)	104.802	111.855	180	179.674	9.602	179.776	18.641
MB	1 (-op)	105.554	111.465	180	-176.895	-6.259	-177.972	18.670
IAA	1.3 (-op)	105.083	111.709	180	-179.262	11.330	179.599	18.632
SPA	1.3 (-op)	104.771	111.871	180	179.025	-8.581	-178.499	18.859
BA	1.3 (-op)	104.281	112.127	180	-179.981	10.114	-179.707	18.574
EL	2 (-op)	103.789	112.385	180	-179.80	13.447	178.626	18.605
PO	4 (-op)	105.442	111.523	180	-176.578	15.857/ -54.220	179.327	18.649
GA	2 (op)	104.471	112.028	180	-178.542	-18.122	179.532	18.586
MF	4 (-op)	105.393	111.548	180	-178.553	-13.097	178.373	18.664
EG	2.6 (-op)	103.712	112.425	180	175.562	26.803	-177.575	18.612

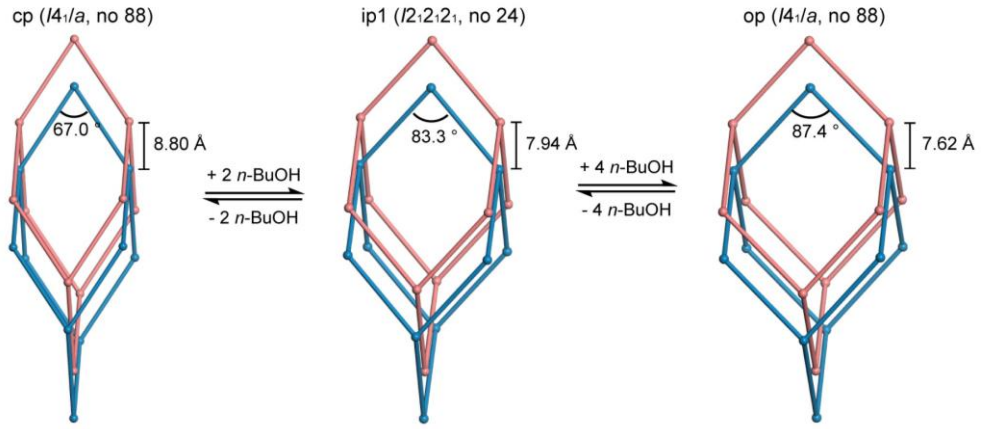

Figure S58. The variation of the angle between the topology nodes.

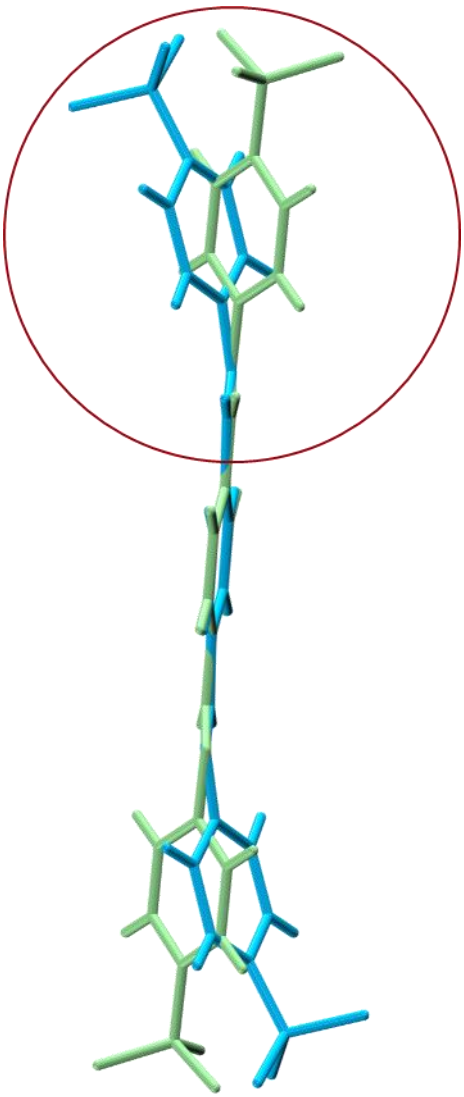

Figure S59. Visualized comparison of different ψ torsion angles between COF-300-cp (blue) and COF-300-op (green).

Section 5. *In-situ* PXRD during dynamic vapor sorption

In-situ PXRD patterns during dynamic vapor sorption were collected on a Bruker D8 advance diffractometer operated at 40 kV and 40 mA with Cu Kα radiation (λ = 1.5418 Å). The sample was loaded into an XRK-900 stage reaction chamber. To ensure the pure activated phase of COF-300 before *in-situ* PXRD experiments, Dynamic vapor sorption (DVS) isotherms and cycling water uptakes were collected on a Surface Measurement Systems Resolution gravimetric DVS instrument, demonstrating the hydrated sample can be activated under N_2 flow. Therefore, before the diffraction experiments, the sample was heated to 60, 80, 120, and 150 °C for activation with a N_2 flow rate of 200 mL/min.

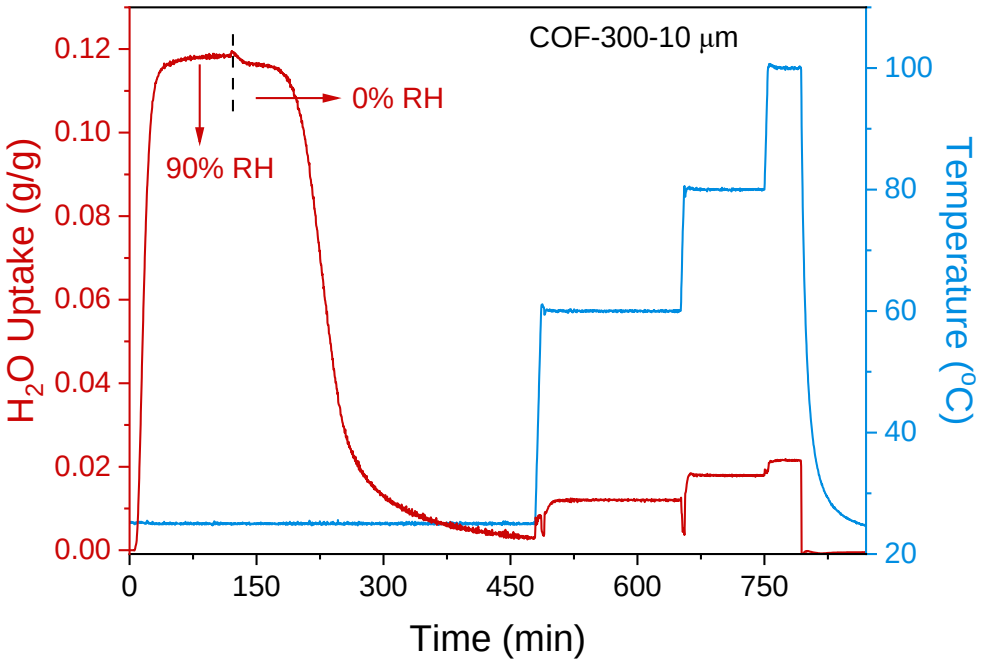

Figure S60. Water adsorption and desorption at variable temperatures tested by a dynamic vapor sorption (DVS) analyser under N_2 atmosphere, showing water can be desorbed completely from COF-300 at 100 °C.

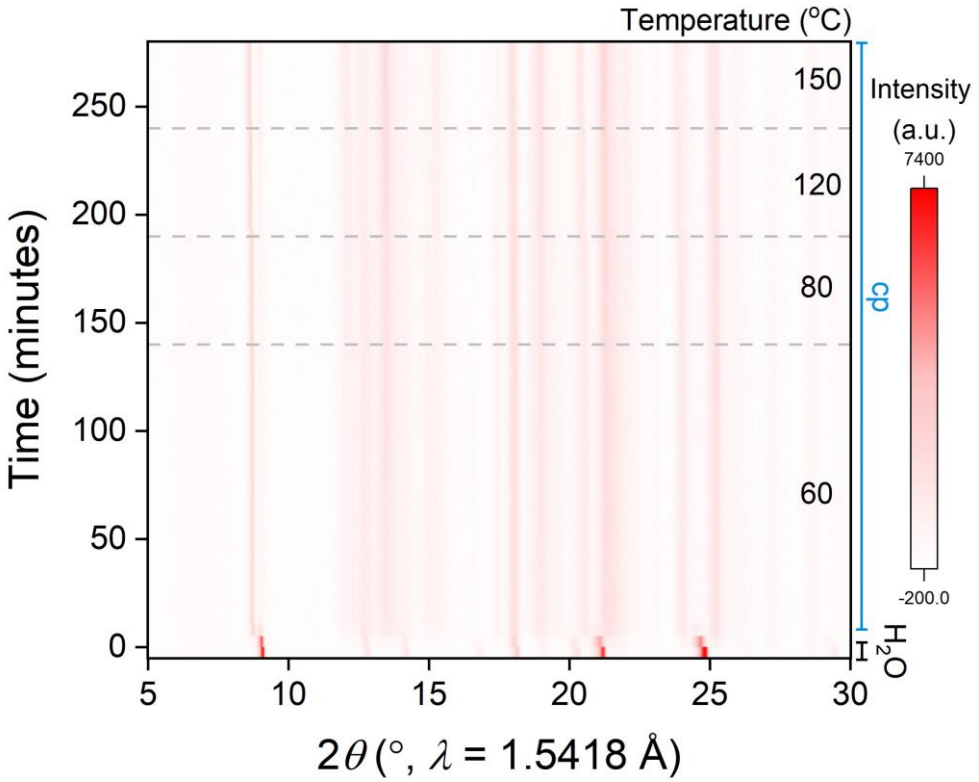

Figure S61. Contour plot of the *in-situ* PXRD during heating hydrated COF-300 under N_2 atmosphere. While undergoing *in-situ* heating at 150 °C under a protective N_2 atmosphere, the PXRD pattern reveals a peak within the aqueous phase, suggesting the presence of crystal memory effects.

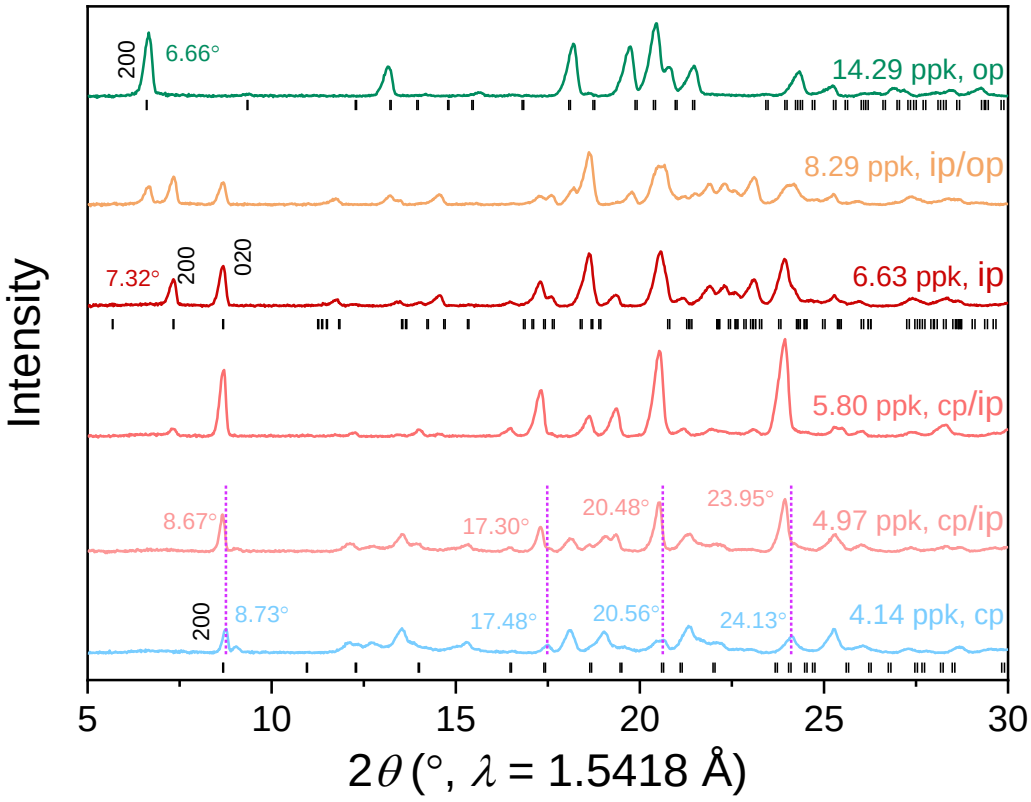

Figure S62. Comparison of PXRD patterns of equilibrium states during *n*-BuOH adsorption at 302 K, showing the structural transition upon *n*-BuOH inclusion.

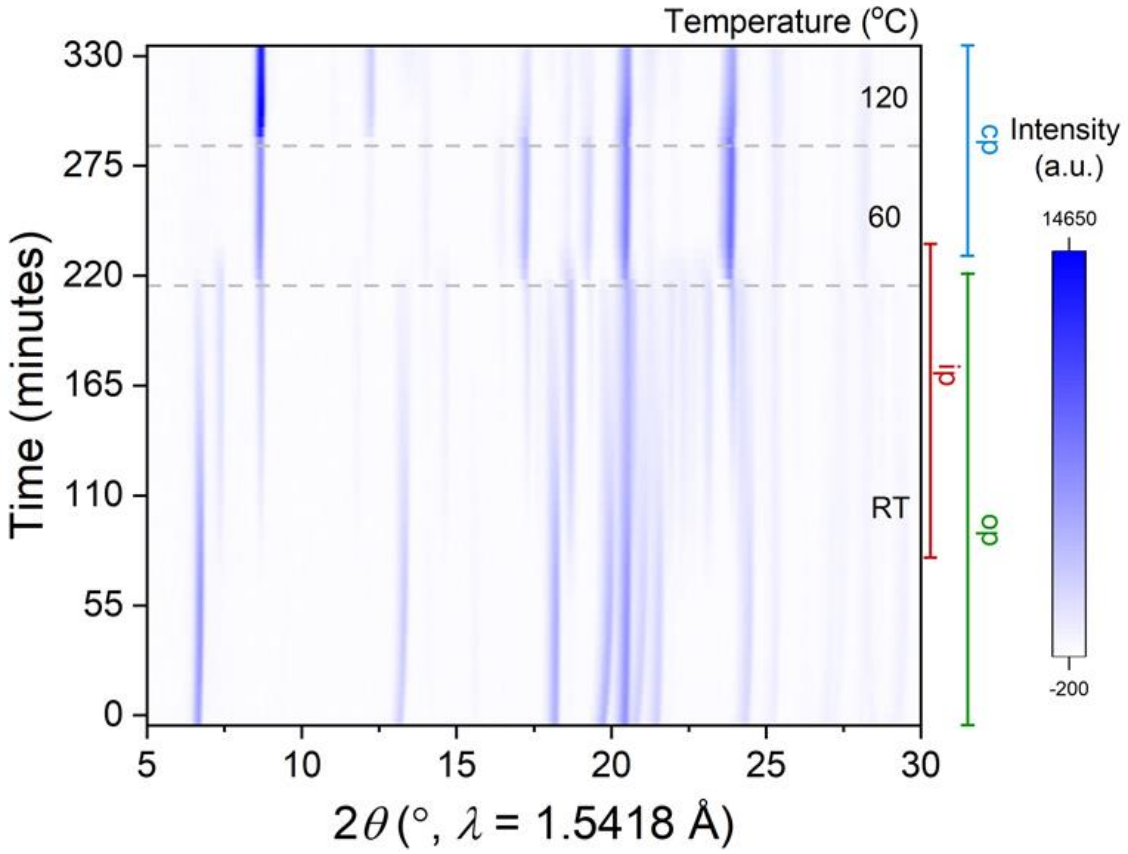

Figure S63. Contour plot of the *in-situ* PXRD during heating COF-300 for tracing its intermediate phase at variable temperatures under N_2 atmosphere. Initially, the structure was purged with N_2 at room temperature, presenting a mixed phase of COF-300-op and -ip. Upon heating to 60 °C, COF-300-op vanished. Subsequently, when raised to 120 °C, the structure underwent a reversible transformation to a crystalline COF-300-cp.

Section 6. Theorical calculation and molecular simulation

Panoramic View of Conformational Energy: The conformational search are Molclus software[2] was used to calculate the different conformational phase single-point energy using MMFF44 force filed[3] embedded Open Babel software[4].

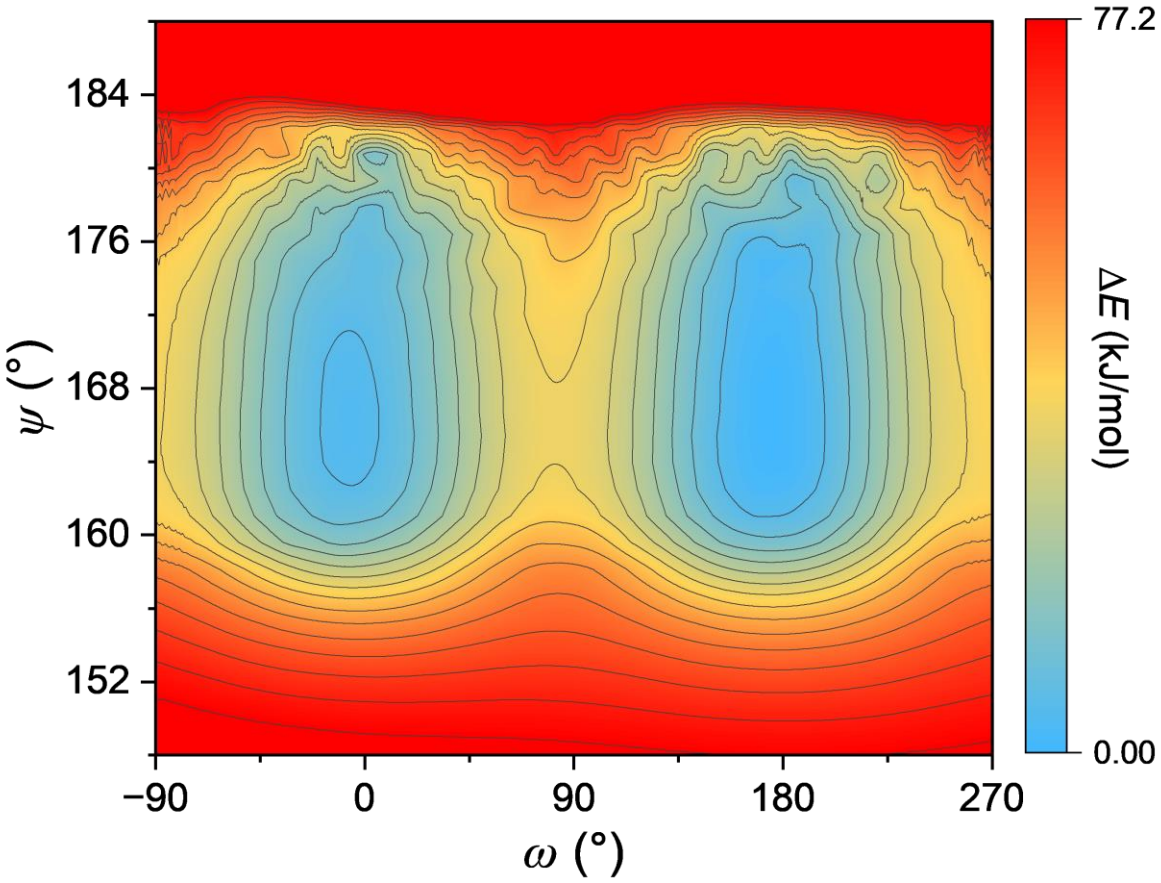

Figure S64. The rotational energy landscape of COF-300 rotamers

Independent gradient model based on hirshfeld partition of molecular density (IGMH) analyses. The independent gradient model based on Hirshfeld partition of molecular density (IGMH) method[5] reported by Lu et al. in 2022 was used to explore the framework-framework interactions. IGMH method is an improved version of independent gradient mode (IGM)[6], which replaces the free-state atomic densities involved in the IGM method with the atomic densities derived by Hirshfeld partition of actual molecular electron density.

The $\boldsymbol{\delta g}$ function are defined as the difference between IGM type of density gradient ($\boldsymbol{g^{IGM}}$) and the gradient of promolecular density ($\boldsymbol{g}$). This parameter has a positive correlation with the strength of intermolecular interactions within an interatomic interaction region and can thus be used to measure the relative strength of these interactions[7].

The intermolecular interactions can be expressed as[5]

$$\boldsymbol{\delta g^{inter}(r) = g^{IGM,inter}(r) - g^{inter}(r)}$$

with

$$\boldsymbol{g^{inter}(r) = \left| \sum_{A} \sum_{i \epsilon A} \nabla \rho_i^{free}(r) \right|}$$

where $\boldsymbol{r}$ represents the Cartesian coordinate vector, $\boldsymbol{A}$ loops over all fragments, $\boldsymbol{i}$ loops all atoms in the corresponding fragment and $\boldsymbol{\rho_i^{free}}$ represents the spherically averaged density of atom $\boldsymbol{i}$ in its free state.

The IGMH analyses are CP2K software[8] was used to conduct the DFT calculations to get the wavefunction files using PBE[9]-D3(BJ)[10] exchange-correlation density functional with the DZVP-MOLOPT-SR-GTH basis set[11].

Intercepting the adjacent two-fold structure of the four COF-300 links for IGM calculations, we focus only on the intermolecular interactions, denoted as δg-inter. and decompose the inter-framework interactions into the contribution of each atom, denoted as δg-index, the larger the δg-index, the larger the contribution of the atom to the interactions. And VMD is used to colour the atoms by δg-index to show the structure.

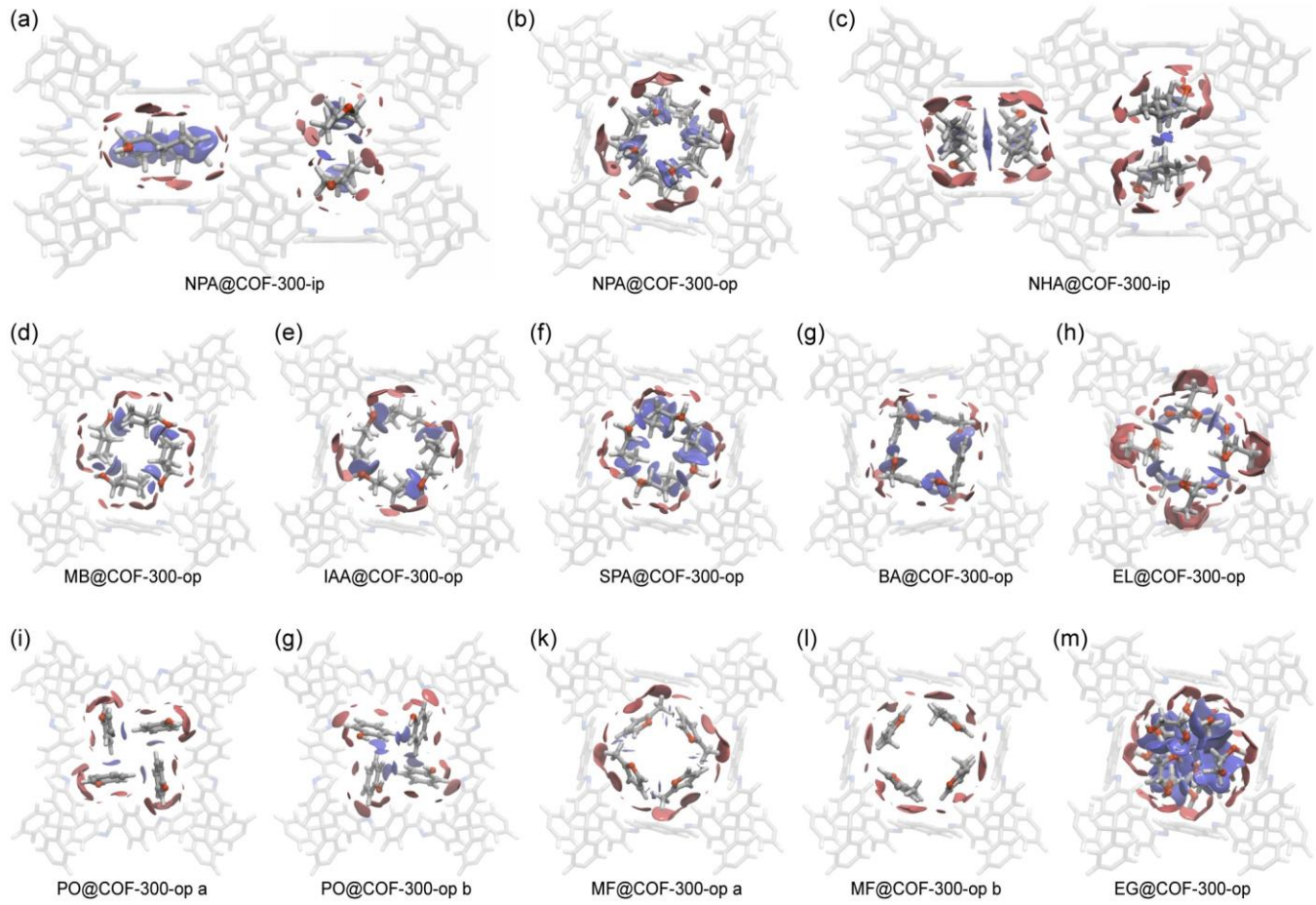

Figure S65. *Sign(λ_2)ρ* coloured isosurfaces of δg^{inter} = 0.005 a.u. of host-guest (colored red) and guest-guest (colored blue) interactions via IGMH method for different dynamic confinement space COF-300. (*n*-Pentanol, NPA; *n*-Hexanol, NHA; 2-Methyl-n-butanol, MB; Isoamyl alcohol, IAA; 2-Pentanol, SPA; Benzyl alcohol, BA; Ethyl lactate, EL; Phenol, PO; 2-Methylfuran, MF; Ethylene glycol, EG)

Single-point energy calculation: The single-point energy calculations are CP2K software[8] was used to conduct the DFT calculations to get the wavefunction files using B97m-rV[12] exchange-correlation density functional with the pob-DZVP-rev2 basis set[13].

Table S22. Relative energy of COF-300 at -cp, -ip and -op phase without guest molecules.

Relative Energy	-cp	-ip	-op
ΔE_H (kJ/mol)	0	43	61
$\Delta E_{H\text{-}G}$ (kJ/mol)	0	-107	-134

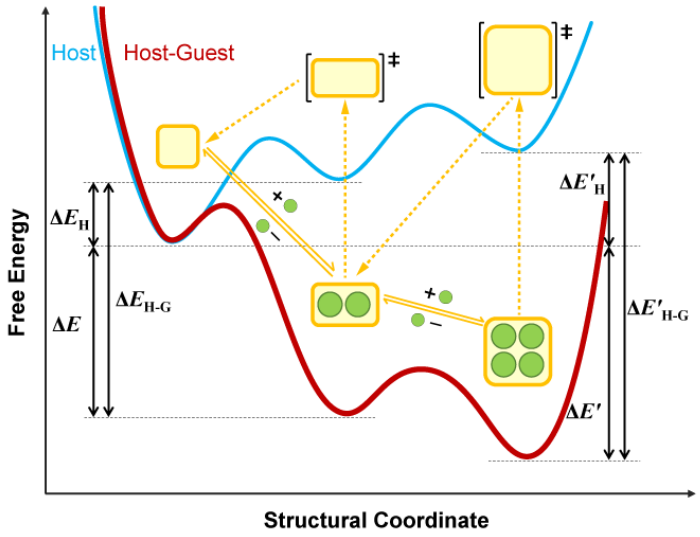

Figure S66. The energy pathway of the structure transformation of COF-300 from -cp to -ip and -op.

References

S1. Sheldrick, G.M. A short history of SHELX. *Acta Cryst*. **2008**, *A64*, 112.

S2. Lu, T. Molclus Program, Version 1.12, http://www.keinsci.com/research/molclus.html (accessed Nov 6, 2024)

S3. (a) Halgren, T. A. Merck molecular force field. I. Basis, form, scope, parameterization, and performance of MMFF94. *J. Comput. Chem*., **1996**, *17*, 490-519. (b) Halgren, T. A. Merck molecular force field. II. MMFF94 van der Waals and electrostatic parameters for intermolecular interactions. *J. Comput. Chem*., **1996**, *17*, 520-552. (c) Halgren, T. A. A. Merck molecular force field. III. Molecular geometries and vibrational frequencies for MMFF94. *J. Comput. Chem*., **1996**, *17*, 553-586. (d) Halgren, T. A.; Nachbar, R.B. Merck molecular force field. IV. conformational energies and geometries for MMFF94. *J. Comput. Chem*., **1996**, *17*, 587-615. (e) Halgren, T. A. Merck molecular force field. V. Extension of MMFF94 using experimental data, additional computational data, and empirical rules. *J. Comput. Chem*., **1996**, *17*, 616-641

S4. O'Boyle, N.M.; Banck, M.; James, C.A. Morley, C.; Vandermeersch T.; Hutchison, R.H. Open Babel: An open chemical toolbox. *J Cheminform,* **2011**, *3*, 33

S5. Lu, T.; Chen, Q. Independent gradient model based on Hirshfeld partition: A new method for visual study of interactions in chemical systems. *Journal of Computational Chemistry* **2022**, *43* (8), 539-555.

S6. Lefebvre, C.; Khartabil, H.; Boisson, J.-C.; Contreras-García, J.; Piquemal, J.-P.; Hénon, E. The Independent Gradient Model: A New Approach for Probing Strong and Weak Interactions in Molecules from Wave Function Calculations. *ChemPhysChem* **2018**, *19* (6), 724-735.

S7. Lefebvre, C.; Rubez, G.; Khartabil, H.; Boisson, J.-C.; Contreras-García, J.; Hénon, E. Accurately extracting the signature of intermolecular interactions present in the NCI plot of the reduced density gradient versus electron density. *Physical Chemistry Chemical Physics* **2017**, *19* (27), 17928-17936.

S8. Kühne, T. D.; Iannuzzi, M.; Del Ben, M.; Rybkin, V. V.; Seewald, P.; Stein, F.; Laino, T.; Khaliullin, R. Z.; Schütt, O.; Schiffmann, F.; et al. CP2K: An electronic structure and molecular dynamics software package - Quickstep: Efficient and accurate electronic structure calculations. *The Journal of Chemical Physics* **2020**, *152* (19), 194103.

S9. Perdew, J. P.; Burke, K.; Ernzerhof, M. Generalized Gradient Approximation Made Simple. *Phys Rev Lett* **1996**, *77* (18), 3865-3868.

S10. Grimme, S.; Ehrlich, S.; Goerigk, L. Effect of the damping function in dispersion corrected density functional theory. *J Comput Chem* **2011**, *32* (7), 1456-1465.

S11. VandeVondele, J.; Hutter, J. Gaussian basis sets for accurate calculations on molecular systems in gas and condensed phases. *The Journal of Chemical Physics* **2007**, *127* (11).

S12. Narbe M.; Luis Ruiz P.; James C. W.; Chris-Kriton S.; Teresa H-G.; Martin Head-Gordon. Use of the rVV10 Nonlocal Correlation Functional in the B97M-VDensity Functional: Defining B97M-rV and Related Functionals. *J. Phys. Chem. Lett*. **2017**, *35* (8)

S13. Daniel Vilela O.; Joachim L.; Michael F. P. Thomas B. BSSE-Correction Scheme for Consistent Gaussian Basis Setsof Double-and Triple-Zeta Valence with Polarization Qualityfor Solid-State Calculations. *J. Comput. Chem*. **2019**, *2364* (40)